DESIGN AND CHARACTERIZATION OF LOW TEMPERATURE CO-FIRED CERAMIC DIELECTRIC BARRIER DISCHARGE PLASMA ARRAYS FOR KILLING AND REMOVING BACTERIAL BIOFILMS

by

Adam Croteau

A thesis

submitted in partial fulfillment

of the requirements for the degree of

Master of Science in Electrical and Computer Engineering

Boise State University

August 2020

© 2020

Adam Croteau

ALL RIGHTS RESERVED

BOISE STATE UNIVERSITY GRADUATE COLLEGE

DEFENSE COMMITTEE AND FINAL READING APPROVALS

of the thesis submitted by

Adam Croteau

Thesis Title: Design and Characterization of a Low Temperature Co-Fired Ceramic Dielectric Barrier Discharge Plasma Array for Destroying and Removing Biofilms

Date of Final Oral Examination: 10 July 2020

The following individuals read and discussed the thesis submitted by student Adam Croteau, and they evaluated their presentation and response to questions during the final oral examination. They found that the student passed the final oral examination.

Jim Browning, Ph.D.	Chair, Supervisory Committee
Ken Cornell, Ph.D.	Member, Supervisory Committee
Don Plumlee, Ph.D.	Member, Supervisory Committee

The final reading approval of the thesis was granted by Jim Browning, Ph.D., Chair of the Supervisory Committee. The thesis was approved by the Graduate College.

DEDICATION

I would like to dedicate this document to my parents and sister who without their continued support and encouragement, none of this would be possible.

ACKNOWLEDGMENTS

I would like to thank my committee faculty members for their guidance, expertise and the occasional swift kick to keep the ship pointed straight. Thank you to Amanda White and Jacob Tenorio, whose skill and art in the construction of the devices was paramount to the success of the project, and Drake Sanborn and Michael Okebiorun for help in running experiments. I'd also like to thank the bio team members (Dalton Miller, Spencer Goering, Mariah Provost, and Tyler Smith) for their assistance in training the engineers how to grow and safely handle biologicals.

Thank you to Dupont for their generous donation of 951 Low Temperature Co-Fired Ceramic materials with which all these devices are constructed.

Thank you to the National Institute of Health (NIH) and U.S. Department of Agriculture (USDA) for the opportunity to pursue this research project under the following grants, NIH # 1R15EB024930-01A1, USDA #2018-67018-27881, USDA # 2020-67018-30789.

ABSTRACT

Present research at Boise State University (BSU) has demonstrated the ability of low temperature co-fired ceramic (LTCC) Dielectric Barrier Discharge (DBD) cold atmospheric pressure plasma (CAP) devices to remove bacterial biofilms on steel substrates. Although bacteria may easily be inactivated by plasma treatment, the remains of the organism are still present on the substrate. It is shown that single element DBD CAP discharge devices operating at 2100 Vrms with 5 LPM of hydrated argon gas etched *P. fluorescens* biofilm within a few minutes of exposure. Similarly, using an 8 element array of linear plasma discharges, etch removal of biofilm was demonstrated. After 5 minutes of treatment, the majority of the biofilm was removed leaving only a thin layer (≈8 µm) remaining. Incorporating 150 kΩ ballast resistors in multi-discharge arrays greatly reduced variation in discharge channel current. The thermal properties of these devices were also determined in order to find optimal gas flow rates to prevent killing biofilm bacteria by thermal processes. This research shows that feed gas flow rates, power delivered to the plasma, proximity to substrate and flow gas hydration are important factors in etching or removal of bacterial biofilms from surfaces.

TABLE OF CONTENTS

DEDICATION iv

ACKNOWLEDGMENTS v

ABSTRACT vi

LIST OF FIGURES ix

LIST OF ABBREVIATIONS xvi

CHAPTER ONE: INTRODUCTION AND BACKGROUND 1

Introduction 1

Background 2

CHAPTER 2: APPARATUS AND SYSTEMS OVERVIEW 8

Single Linear Discharge Device Overview 8

Multiple Discharge Array Device Overview 13

Device Design and Fabrication 15

Biofilm Preparation 18

CHAPTER 3: EXPERIMENTAL PROCEDURE 22

CHAPTER 4: DEVICE CHARACTERIZATION 25

Characterization of DBD Single Linear Discharge Devices 25

Characterization of DBD Multiple Discharge Plasma Arrays 35

CHAPTER 5: CAP TREATMENT OF BACTERIAL BIOFILMS 50

Overview 50

Etching with Single Linear Plasma Discharges 54

Etching with DBD Plasma Arrays 60

CHAPTER 6: SUMMARY AND CONCLUSION 64

Summary of Results and Discussion..64

Conclusion 65

Future Work 66

REFERENCES 67

LIST OF FIGURES

Figure 1. Reflection in glass of an ambient air pre-stable DBD CAP formed between the discharge electrodes (indicated by the yellow arrow) within the gap at 1.2 kV, no gas flow. (Left) t=0 s. (Right) t=3 s. Notice the changing bright spots over time. This is a typical single linear discharge device used for this research. 4

Figure 2. Percentage remaining CFU's after treatment with linear discharge plasma device. These experiments were run with Staphylococcus aureus (top) and nonpathogenic E. coli BL-21 2-day old biofilms (bottom). Shown here are the CFU counts of Staphylococcus aureus and E. Coli. The gas control consists of an equivalent treatment of bacterial biofilm with only carrier flow gas and no plasma discharge. 7

Figure 3. Schematic of a single channel plasma system. A 50 V/A current transformer is used to measure the discharge current and a Cal Test CT2982B High voltage probe (7 kVrms max, 40 MHz BW) measures voltage across the discharge to ground. Shown in blue is the LTCC with embedded electrodes, between which the plasma is generated. Mass flow controllers regulate the flow of oxygen and argon into the discharge gap and direct the flow of ions out of the device [20]. 8

Figure 4. Close up diagram of the plasma device. Note the layers of LTCC. The embedded electrodes are created with silver paste built into the LTCC with a 5-mil cover sheet on top of each electrode. 9

Figure 5. (Left) Dimensions of LTCC high voltage (HV) and low voltage (LV) plate. (Right) Dimensions of LTCC spacer plates. 10

Figure 6. Layout of individual sheets required for making a single LV plate with built in ballast resistors. The top left sheet with embedded ballast is actually reversed just to show the resistor. During assembly this sheet would be flipped so that the ballasts are both facing out. This allows us to put two HV plates on either side creating a 2x array. The black arrows indicate the pre-fire ballast resistors. 11

Figure 7. (Left) Circuit diagram of the standard setup with ballast resistor on the groundside. (Right) Setup with a ballast resistor on the HV side. 12

Figure 8. (Top) Facing outwards, the 3D printed gas nozzle is epoxied to the gas porthole. (Bottom) Shown here is the inside of the device. On the front piece (bottom left), the high voltage line can be seen running down to the discharge channel. Also shown is the Double Sided Electrically Conductive Adhesive sheets by NISSHIN EM CO. LTD. The conductive sheets are used to connect the via holes together. The backside piece (bottom right) is the groundside piece and the trace is on the opposite side of the assembly to minimize capacitive coupling of the traces. The two trace pieces are separated by a 0.5 mm (20 mil) shim designed to channel the gas flow into the discharge channel. 13

Figure 9. Top: 8 element DBD Array. The left header pin is the HV side and the right pin is the ground side. Bottom: Circuit of a 3x array. Shown here is Cp, Rp and Rb which are respectively the plasma capacitance, the plasma resistance and the ballast resistance. Additional discharges are simply stacked onto the existing assembly. 14

Figure 10. SOLIDWORKS Assembly of a 4x array showing how each piece from Fig. 8 is stacked together to form an array structure................................ 15

Figure 11. (Left) Five layers of 10 mil (0.254 mm) and one 5 mil layer LTCC drawn in CorelDRAW12. The + marks are fiducial holes used for alignment during fabrication. The four holes in the corners are used as screw holes for final assembly securement and mounting in the experiment setup. The center hole serves as the gas feed hole. Two 5 mil layers are used as the conductor cover sheet. This serves to protect the silver trace from oxidation during operation. The four square via holes are probe locations for measuring resistance in devices with embedded resistors. The two small holes in the corners are via holes for connecting the trace to headers mounted after final assembly. (Right) These two pieces are printed on photo paper and are used to sandwich the assembled piece in the press. The small holes are used to align the stack while being pressed. It has been found that without these pieces the assembly can stick to the press and pull apart.. 17

Figure 12. Furnace heat cycle for each stack of LTCC. 18

Figure 13. (Left) Image taken via Bruker Stylus Profilometer. The bottom half of the image is the steel substrate and the top half is P. fluorescens. The crosshairs indicate where the stylus (triangular shadow shown) will begin the scan. The blue arrow indicates the scan direction (Right) Shown here is the profile of the biofilm. It can be seen that the edge is the thickest part of the biofilm. This is consistent across all samples as this is where the sample submerged in LB broth meets the air. This is referred to as the oxygen boundary layer or O2 boundary. In this sample, the biofilm is about half a micron thick. This is a problem that will be addressed in

Chapter 5 as it is preferred to have much thicker biofilms (≈10 μm). The negative value comes from an F operator function that helps to level the sample data.......... 20

Figure 14. Pretreatment P. fluorescens biofilm on stainless steel substrate indicated by the blue arrow. Typically P. fluorescens film thickness is on the order of 2-15 um. This image shows the biofilm after being dipped in DI water according to the experimental procedure outlined in Chapter 3.......... 21

Figure 15. Photograph of a single linear discharge CAP device with and without gas flow. (Left) No Ar gas flow (Ambient air) at 2 kV. (Right) 5 LPM Ar gas flow at 900 V. Notice the stability and uniformity of the discharge.......... 26

Figure 16. Photograph of multi-gas discharge operating at 2 kV with 5 LPM Ar flow through the center of the discharge with ambient air discharges on the edges. Note the stability of the discharge even when under multiple gas flow conditions.......... 26

Figure 17. The red trace is the IV of a single linear discharge device with 5 LPM Ar gas flow. In blue is the IV when no Ar gas is flowing through the device. The line fits are used to determine the equivalent resistance of the device while operating.......... 27

Figure 18. Magnitude Vrms vs frequency for 5 LPM Ar flow and 0 LPM (Ambient air). The starting points were selected based on the upper threshold for safely operating the device. At voltages >2 kVrms with Ar flow, the discharge begins audible cracking due to the intensity. Gap width =20 mil (0.508 mm).......... 29

Figure 19. Corresponding current and voltage waveforms for Fig. 17. (Left) No argon flow. (Right) 5 LPM argon flow. The current readings are 10x higher than actual because the Agilent DSO5014A oscilloscope did not have a 50 V/A setting Therefore a reading of 23.02 mA actually is 2.302 mA. Note the current waveform shows the distortion from the plasma.......... 31

Figure 20. Current vs voltage plots of Argon gas flow and no gas flow. The circled section is magnified and shown in Fig. 21. The arrows indicate which direction the voltage is changing i.e. increasing then decreasing.......... 31

Figure 21. Magnified current vs voltage plot of 5 LPM Ar flow.......... 32

Figure 22. Thermogram of single linear discharge plasma device operating at 5 LPM Ar flow, 2 kV and 2.3 mA after five minutes of exposure. The gap between the electrodes is 1.2 mm and the device is 3 mm above the substrate. The temperature range shows the maximum and minimum

temperature in the image to be 29.4°C and 23.6°C respectively. The steel heats only to 25°C which is far below the 35°C threshold. 34

Figure 23. Photographs of typical arcs from a single linear discharge device. (Left) Treatment settings: 1.6 kV, 1.2 mm gap, 1 mm to substrate, 5 LPM Ar, external ballast 100 kΩ. A small arc to substrate is shown circled. (Right) 4 kV, 1.2 mm gap, 5 mm to substrate, 5 LPM Ar. These are typical arcs seen when the discharge channel is brought too close to the treatment surface or ground chuck. 35

Figure 24. Photograph of an 8 element internal ballast resistor array 'A1' from Fig. 8 operating at 900 V, 9.5 mA with 9 LPM Ar flow. 36

Figure 25. Photograph of a test array with isolated channels. (Right) A five channel array constructed so that each discharge channel is isolated from one another. This allows for independent channel selection and IV characteristics in situ. (Left) The center discharge of the test array operating at 4 kV without gas flow with 100 kΩ ballast. 37

Figure 26. IV data for 1 kΩ, 100 kΩ and 200 kΩ external ballast resistors with 5 LPM Ar flow gas. The 1 kΩ data lacks an 1100 V data point due to significant channel to channel arcing beginning to occur. The arrow pointing down indicates an element that developed a bright spot. The arrow point up indicates an element that exhibited a fabrication defect... 38

Figure 27. Averaged data points from Fig. 26. This is a cleaner visualization of the effects of the external ballast resistor. 39

Figure 28. Photograph of a single HV line igniting a weaker stable plasma in the second channel and a transient plasma in the third via capacitive coupling. Since each channel is electrically isolated, it is the capacitance of the LTCC that the voltage on channel 1 is coupling through. This occurs at >3.5 kV for this device with 5 LPM of Ar flow. 40

Figure 29. IV comparison between coupled and isolated channels, both with 100 kΩ ballast resistors. Clearly there is a difference in behavior between multi-discharge arrays and single discharge devices in an array configuration. This represents a drop in equivalent resistance from 750 kΩ to 440 kΩ.. 42

Figure 30. Thermogram over time for an 8x Array operating at 2 kv with 9 mA and no flow gas. The orange arrow points to a small LTCC piece attached to the device that sets the proximity to the substrate. After 5 minutes the substrate remains safely below the thermal kill threshold. 43

Figure 31. Thermogram of 8x Array at 2 kV after 5 minutes with 6 LPM Ar. From the spot measurements, it is clear that the plasma is much more intense (39.8°C) than that of Fig. 30 (32.5°C) where no gas was flowed. Though more convective heat transfer is taking place via gas flow, the intensity of the plasma causes the substrate to heat up beyond the thermal kill threshold. The amount of heat removed from the substrate via gas flow is unable to keep up with the rate of heat delivered. 44

Figure 32. Thermogram of 8x array at the operating conditions outlined in Fig. 31 except with 13 LPM of Argon gas flow. After 5 minutes the substrate is well below the kill threshold at 33.5°C. It can also be seen the device itself remains much cooler throughout the treatment cycle via the max reading on the right side of the figure. 45

Figure 33. Schematic of a 3x array with parallel inductance Lr. 46

Figure 34. Pre-ignition waveform with parallel inductance. 33.6 kHz is the resonant peak. Note that the current is 0.1x RMS(2) = 1.7 mA. 47

Figure 35. Current and Voltage waveforms of an 8x array with resonant inductance. Similar to Fig. 19, there is similar distortion on the current waveform. However, the noticeable difference is that in Fig. 19 the noise occurred after the peak of the sinusoid. Whereas with the resonant inductor the noise occurs pre-peak. The new operating resonant frequency is 25.5 kHz as shown. 48

Figure 36. A typical arc generated from an 8x array to a grounded substrate. This particular device arcs at 1500 V at 4 mm to the substrate with 5 LPM Ar. 49

Figure 37. Various organisms CFU counts at specified treatment times at 1800 V and 5 LPM Argon gas flow through single linear discharge. Additional results will be presented in upcoming papers. 51

Figure 38. The effect of 10.2 LPM hydrated argon gas flow for 5 minutes through an 8 element array with no plasma. (Top) Microscope image of P. fluorescens on steel. The right hand section is steel substrate and the left shows the discolored bulk biofilm. The yellow arrow points to the areas without biofilm. Clearly, the underlying substrate lines are visible through the biofilm. (Bottom) Profilometer scan of the Top image from left to right. It can be seen that the bulk biofilm is approximately 2 μm even when translucent. This effect only occurs when flowing hydrated gas through the device. 53

Figure 39. P. fluorescens biofilm control with no gas or plasma treatment. The green regions indicate the dried biofilm. The bottom right of the image indicates the steel substrate. 54

Figure 40. Control test of P. fluorescens with 8 LPM Hydrated Ar for 4 min at 3 mm and no plasma. The large yellow arrow points the boundary between steel substrate on the right and translucent biofilm on the left. The yellow box indicates the orientation of the device above the substrate and outlines a top and bottom boundary of plasma treatment. The plasma discharge above the sample extends off the right and left edges of the box beyond the extent of the image indicated by the small white arrows. 55

Figure 41. 3100 V, 3.1 mA at 3 mm for 4 min with 8 LPM hydrated Ar. There is significant displacement of biofilm occurring in the oxygen boundary. The bulk biofilm however remains intact. The yellow box indicates the placement of the plasma device over the sample similar to Fig. 40. The device extends off the left and right edges of the box. The yellow arrow indicates the orientation of the scan in Fig. 42. 56

Figure 42. Profilometer scan of Fig. 41. Clearly the first 6 mm is steel substrate before encountering the biofilm oxygen boundary. At 10 mm there is a spike from either biofilm or foreign debris. 57

Figure 43. Plasma treatment of 3100 V, 3.1 mA at 3 mm for 4 min with 9 LPM hydrated Ar. The yellow box indicates the placement of the plasma device over the P. fluorescens sample. The device extends off the left and right edges of the box indicated by the small white arrows. 57

Figure 44. 10 minute treatment at equivalent treatment conditions to that of Fig. 41. The yellow box indicates the orientation of the plasma device above the substrate. 58

Figure 45. Etching occurring in the oxygen boundary as well as the bulk regions. (Left) the bulk region shows significant etching. (Right) the etched oxygen boundary has a significantly wider etch area than the bulk. The larger yellow arrows point to the same etch region where the images would overlay. The yellow box indicates the approximate width of the discharge above the sample, extending off the left and right edges of the image indicated by the small white arrows. 59

Figure 46. Scan of Fig. 45 (Left) from the center of the etched region to the top of the figure. This shows an approximate 4 μm of etch over 4 minutes or an etch rate of 1 μm/min. 59

Figure 47. Pre-treatment control and post-treatment of a P. fluorescens biofilm on stainless steel. (Left) Control with 12 LPM of Ar gas for 5 minutes. The

oxygen boundary is the bottom of the image and the device is oriented vertically above indicated by the double yellow arrow. (Right) Post-treatment with 1600 V, 9.8 mA at 5 mm with 12 LPM dry Ar for 5 minutes. The etch region is indicated and can clearly be seen as being removed cleaned down to the steel substrate. 61

Figure 48. (Top) Image of the scan region described in Fig. 47 starting in the etched biofilm bulk and ending just past the O_2 boundary indicated by the yellow arrow (Left to right). The entire region shown was subjected to plasma treatment. (Bottom) Profilometry scan of the top image from left to right. 62

Figure 49. (Top) Striation marks left in the bulk biofilm after treatment outlined in Fig. 47. The spacing of the striations are approximately equal to the width of the plasma discharge in each element. (Bottom) Profilometry scan from right to left across the top image. 63

LIST OF ABBREVIATIONS

BSU	Boise State University
LTCC	Low Temperature Co-Fired Ceramic
CAP	Cold Atmospheric Pressure Plasma
ROS	Reactive Oxygen Species
RNS	Reactive Nitrogen Species
NTP	Non Thermal Plasma
CAD	Computer Aided Design
HV	High Voltage
LV	Low Voltage
P. fluorescens	*Pseudomonas fluorescens*
TTL	Transistor Transistor Logic
DUT	Device Under Test
LB	Lysogeny Broth

CHAPTER ONE: INTRODUCTION AND BACKGROUND

Introduction

Cold atmospheric pressure plasma (CAP) has found novel applications in medicine, food processing, material processing and microelectronics industries [1-17]. Effective sanitization of food processing equipment without the use of harsh chemicals has received increased consumer attention and is consequently desired by the industry [1,2]. CAP has potential to augment or replace current sterilization techniques in food processing, medical and agricultural surfaces, and wound cleaning environments. The methods of plasma generation are as diverse as their application, ranging from torches and plasma jets to the dielectric barrier discharge (DBD); the discharge can be generated via inductive or capacitive means [1-14]. The mechanisms with which plasma destroys bacteria are considered to be a combination of UV exposure, reactive oxygen/gas species along with electric, magnetic and thermal fields [1-5,9,11,18,19]. Currently, non-thermal plasma (NTP) is the preferred method of sanitation in medicine and food processing because it causes the least amount of damage to the treatment surface [1,2,5,9].

Prior research at Boise State University (BSU) has shown that CAP discharges effectively kill bacteria in biofilms on a variety of substrates including glass, plastic, and stainless steel [20]. This research indicates that the removal of biofilm via a reactive etching process and physical sputtering mechanisms is feasible and offers significant sanitary advantages compared to simply killing the bacteria in biofilm and leaving the remains behind. The research presented here characterizes the electrical properties of

single linear discharges and multi-discharge CAP devices, and their ability to remove bacterial biofilms from stainless steel.

Background

The ability of atmospheric pressure plasma to disinfect and sanitize surfaces has been well documented [1,3-5,7-9,17,18]. The mechanisms by which sanitation is achieved has been shown to include UV photons (photodesorption), electric field interactions, thermal interactions, chemical processes, reactive oxygen species (ROS), reactive nitrogen species (RNS) and ionic sputtering [1,3,5,9,17,18,21,22]. ROS and RNS such as O_2^-, H_2O_2, O_3, OH^-, $^{\bullet}OH$, NO are created through charge exchanges known as oligomerization [14], and induce a variety of intracellular and extracellular effects that inactivate the target biological through interactions with the cell membrane, lipids, fatty acids, proteins, and nucleic acids. Many studies have been performed to determine the cellular effects of plasma. The results have shown cell membrane rupture due to ion impacts, DNA mutation through the creation of thymine dimers via UV irradiation, and apoptosis (programmed cell death) [1,3,5,9,15]. Generally, disinfection occurs when the bacterial colony forming unit (CFU) count is reduced to an appreciable log reduction (usually on the order of at least 3-log). At this point the species ability to reproduce is severely reduced and death begins to occur. Sterilization is possible when reactive etching or sputtering mechanisms destroy and remove biofilm or bacteria down to the underlying substrate [9].

To help set a foundation for this research, a brief discussion on the physics behind plasmas is needed. In DBD plasmas, by applying a potential difference across the electrodes separated by an air gap, energy stored in the generated electric field is transferred to the plasma by accelerating charged species [6]. It is understood that

nonthermal plasma exists in thermodynamic non-equilibrium, and a significant difference in electron temperature T_e and gas temperature T_g can occur. Given that electrons have a much smaller mass, momentum, and inertia than ions and gas molecules, the plasma chemistry in NTPs is dominated by electron interactions within the gas medium [15]. In contrast, plasmas operating in thermal equilibrium ($T_e \approx T_g$), share the biological effects between electrons and ion species. In this state, the plasma yields a much higher fraction of ionization (close to 100%) [15], but also generates much higher heat gradients that can damage biological species in the treatment and surrounding areas. Thus, NTPs are much more suited for operating in medical and agricultural applications.

The difference in T_e and T_g is characterized by eqn. (1) [6] [23],

$$\frac{T_e - T_g}{T_e} = \frac{m_g}{4m_e} \left(\frac{\lambda_e e E}{\frac{3}{2} k_b T_e} \right)^2, \tag{1}$$

where m_g is neutral particle mass, m_e is electron mass, $\lambda_e$is electron mean free path, E is electric field intensity, e is elementary charge and k_b is Boltzmann's constant. This equation highlights the fact that as the mean free path decreases (increasing gas pressure) per a given |E|, T_g increases and the difference between T_e and T_g decreases. This behavior is important because if the difference decreases significantly, there is a risk of falling out of non-thermal equilibrium. Even if the discharge is still technically considered non-thermal, there may be increased biological inactivation due to thermal processes that should be avoided for the purpose of determining the impact of the plasma alone on the bacterial biofilm and the biological molecules.

Energy is transferred from electrons to molecules and ions via inelastic collisions. If the electron has enough energy, its collision with a given gas molecule can expel one of the molecule's electrons, ionizing the gas. This electron is then free to ionize another

molecule, and a cascading chain reaction takes place. The reaction continues until the number of free electrons created is equal to the number of free electrons recombining or otherwise lost, wherein the plasma becomes sustainable. This can be seen when the plasma is in the beginning stages of igniting. The applied voltage does not supply a sufficiently large electric field to sustain a stable plasma and is thus, transient in time across the discharge gap. This period is known as “ramp up” and refers to the range of voltage where the plasma has begun to discharge until the plasma is stable across the width of the discharge. Fig. 1 shows the early formation of a DBD plasma in air at t=0 s and t=3 s. The discharge can be seen between two Low Temperature Co-Fired Ceramic (LTCC) plates.

Figure 1. Reflection in glass of an ambient air pre-stable DBD CAP formed between the discharge electrodes (indicated by the yellow arrow) within the gap at 1.2 kV, no gas flow. (Left) t=0 s. (Right) t=3 s. Notice the changing bright spots over time. This is a typical single linear discharge device used for this research.

It is generally understood that larger electric fields and increasing gas flow rates improve a plasma device’s capacity for inactivation of bacterial or fungal samples until a given saturation point [17]. As the electric field intensity |E| increases, the fraction of ionization increases per a given gas flow rate through the discharge. This deposits a greater number of reactive species onto the treatment surface. If |E| continues to increase,

the charged species will begin to be confined to the discharge volume and the majority of species escaping the discharge will be neutral [17]. In addition, if the carrier gas flow rate is too large, the plasma will have insufficient time to ionize and the discharge will weaken. It is, however, presumed that this interaction is one of the primary driving mechanisms for etching and sputtering biofilms. It should be noted that defects in electrode and dielectric covering, along with plasma induced cratering, can create local field gradients within the gap that are much higher than the applied electric field [6,24]. This leads to a preferred ionization path known as a streamer or arc. These arcs effectively short out the plasma and large power densities are generated. This causes the defect to enlarge and eventually destroy the device. Generating a uniform, stable discharge is preferred for device longevity and consistent deposition of charged species to the treatment surface. Streamers may also form between the discharge electrodes and the treatment surface. Over time this will damage the surface and the device, and is not considered a viable method of sanitation.

DBDs are an effective means of generating such stable plasmas under atmospheric pressure and non-thermal conditions [1,4,5,6,7,15]. DBDs generally operate anywhere between 0.5-100 kV and 10-500 kHz, but there have also been examples of microwave (2.4 GHz) DBD's [4]. DBDs essentially introduce a capacitive reactance into the circuit between its associated electrodes where the plasma is generated. Resonant circuitry/matching networks and resistive ballast networks may or may not be necessary given the specific device configuration, power, and thermal requirements [6]. It can be advantageous to use pulsed power supplies with a pulse width on the order of 10 ns to further reduce thermal heating within the device and improve power efficiency [6,17,25]. The capacitance of the device is usually extremely small, on the order of nano or

picofarads with the separating gap on the order of millimeters [1,6,19]. It is, however, difficult to fully optimize a specific device given their multitude of operating parameters. It has been generally determined that crucial process parameters are the type of gas used, the distance to the treatment surface, electrode gap, and the electrical operating point [1517].

There are many materials available for fabricating CAP devices, but one that has gained recent interest is Low Temperature Co-Fired Ceramic [26-30]. LTCC is a ceramic material system that can be machined in its green state. Our specific DuPont 951 LTCC has a dielectric constant of 7.8. It has consistently been proven to excel at integrating meso-scale microsystems [27], such as patch antennas, band pass filters, DNA amplifiers, and an expansive list of sensors [31]. LTCC is extremely flexible in meeting specific substrate design configurations and requirements and has been used in plasma applications [27,29,30]. The ability to be constructed sheet by sheet before firing allows for the design and fabrication of complex 3D structures [28]. This characteristic enables relative ease in fabricating embedding conductive pathways, resistors, and other signal and gas channels within the device.

Prior and ongoing research at BSU has demonstrated the efficacy of using LTCC plasma devices to kill multiple strains of bacteria on a variety of substrates [20]. Prior work has demonstrated the ability of these devices to cause a >3-log reduction in viable CFU’s on the order of 10’s of seconds as shown in Fig. 2.

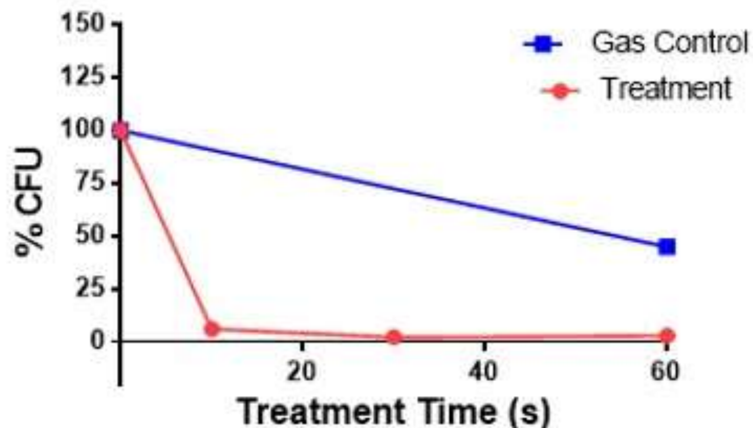

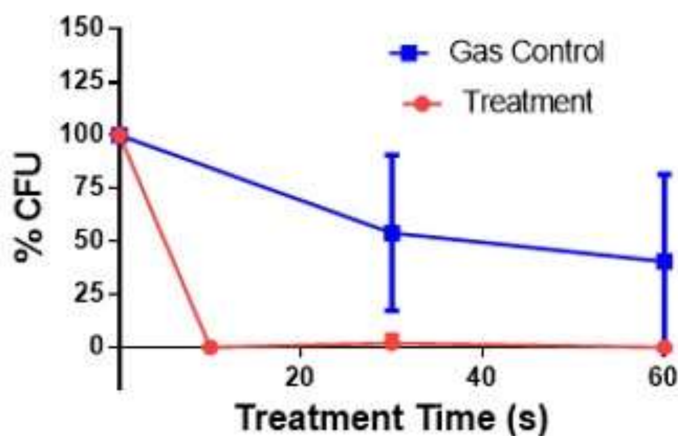

Figure 2. **Percentage remaining CFU's after treatment with linear discharge plasma device. These experiments were run with Staphylococcus aureus (top) and nonpathogenic E. coli BL-21 2-day old biofilms (bottom). Shown here are the CFU counts of Staphylococcus aureus and E. Coli. The gas control consists of an equivalent treatment of bacterial biofilm with only carrier flow gas and no plasma discharge.**

CHAPTER 2: APPARATUS AND SYSTEMS OVERVIEW

Single Linear Discharge Device Overview

Prior research at BSU has demonstrated the ability of a linear discharge plasma device to cause a >3-log reduction in viable cells in biofilms on various surfaces. A general schematic of a single discharge channel device is shown below in Fig. 3 while Fig. 4 shows a diagram of the single discharge plasma device itself. Fig. 4 shows how within the gap, the plasma is generated and the gas flow directs the ions and radicals onto the treatment surface [20].

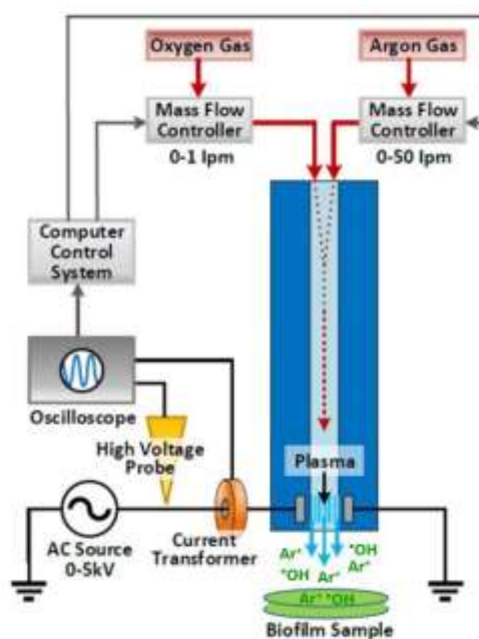

Figure 3. Schematic of a single channel plasma system. A 50 V/A current transformer is used to measure the discharge current and a Cal Test CT2982B High voltage probe (7 kVrms max, 40 MHz BW) measures voltage across the discharge to ground. Shown in blue is the LTCC with embedded electrodes, between which the plasma is generated. Mass flow controllers regulate the flow of oxygen and argon into the discharge gap and direct the flow of ions out of the device [20].

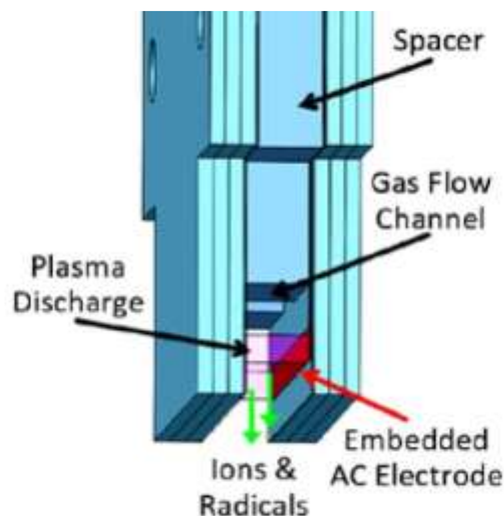

Figure 4. Close up diagram of the plasma device. Note the layers of LTCC. The embedded electrodes are created with silver paste built into the LTCC with a 5-mil cover sheet on top of each electrode.

The distance between the electrodes is referred to as the gap or discharge region, and the distance between the bottom plane of the LTCC to the substrate surface is the proximity. Fig. 5 shows the dimensions of the pieces involved in constructing a single discharge device. These devices are powered by a PVM 500 Plasma Driver from

Information Unlimited (20-40 kHz, 1-40 kV). The Agilent Technologies DSO5014A Oscilloscope monitors the voltage from the HV probe and the current from the current transformer. This oscilloscope lacks a 50 V/A setting so a 5 V/A setting is used and the reported value is 10x higher than actual. Gas flow is controlled via a pair of Kelly Pneumatic KP4541 and KP5866 mass flow controllers for regulating the flow of argon and oxygen, respectively. The gas is then routed through a Dwyer VFA-25 flow gauge for visual calibration and then to a 4L Pyrex gas washing (drechsel) tube filled with deionized water (DI) before entering the discharge channel. The drechsel tube is not shown in Fig. 3 but its purpose is to hydrate the gas before ionization. The impact of the drechsel tube will be described in Chapter 5.

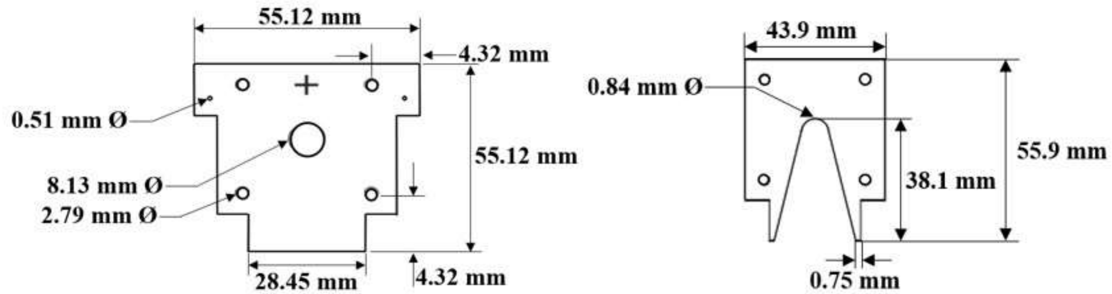

Figure 5. (Left) Dimensions of LTCC high voltage (HV) and low voltage (LV) plate. (Right) Dimensions of LTCC spacer plates.

Resistors are placed in series to the discharge channel in order to control the current through the discharge. These are common in plasma devices and are called ballast resistors. The resistor location on the HV side or LV is important for the deposition of charged species onto the surface and is discussed in Chapter 5. Fig. 6 shows the design of the LTCC sheets with the ballast resistor embedded into the LTCC. While most of the single linear discharge work for this research is conducted with external ballast resistors, multi discharge devices employ embedded resistors. A simple parallel plate capacitance of the element calculation yields approximately 0.4 pF but was measured to be 2 pF per discharge with 0.5 mm gap. Fig. 7 shows a very rudimentary circuit model of the setup under different ballast resistor configurations.

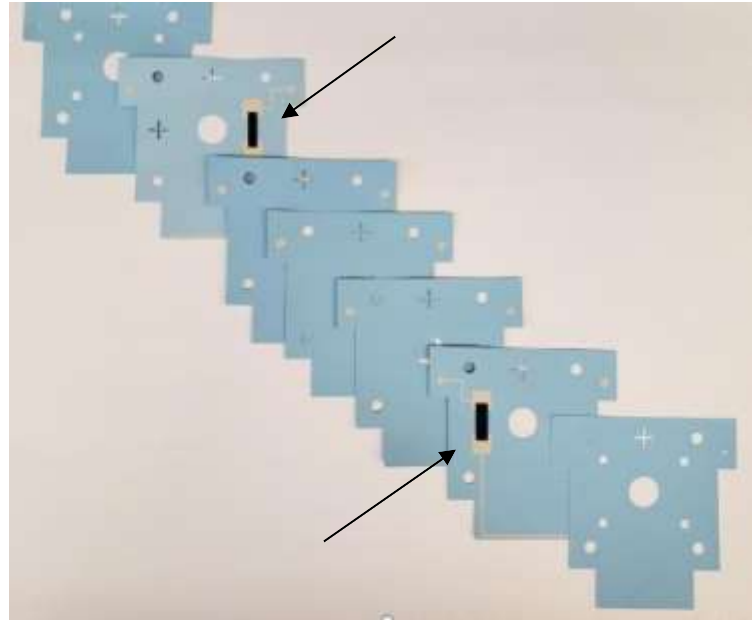

Figure 6. Layout of individual sheets required for making a single LV plate with built in ballast resistors. The top left sheet with embedded ballast is actually reversed just to show the resistor. During assembly this sheet would be flipped so that the ballasts are both facing out. This allows us to put two HV plates on either side creating a 2x array. The black arrows indicate the pre-fire ballast resistors.

The ions and reactive species flow towards a grounded chuck that the substrate rests upon. If the chuck is not grounded, it will float up 100's of volts due to displacement current created by the plasma discharge. This is detrimental to any etching or plasma treatment as any positively charged ions will be repulsed by the relative high potential of the substrate. Under typical operating conditions, there can be anywhere between 50 and 500 volts across the ballast resistor.

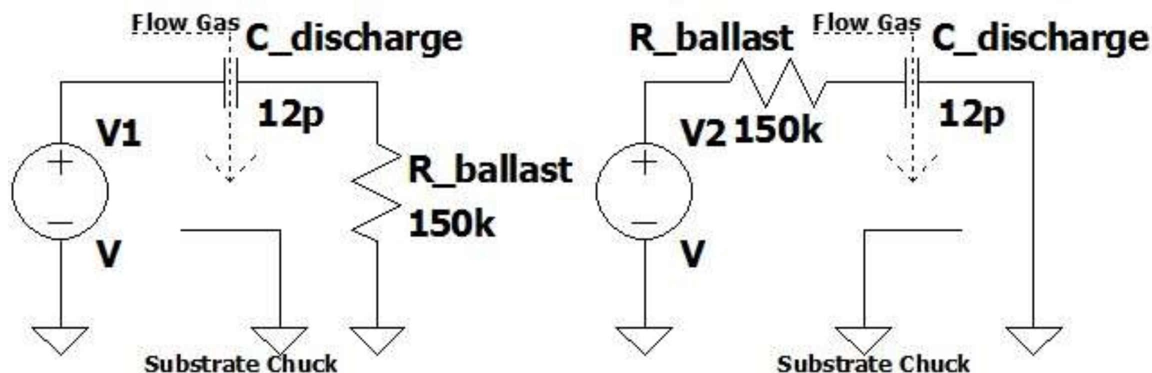

Figure 7. (Left) Circuit diagram of the standard setup with ballast resistor on the groundside. (Right) Setup with a ballast resistor on the HV side.

By moving the ballast resistor to the HV side of the discharge, the device can be moved much closer to the substrate chuck without arcing. Clearly, by moving the ballast to the HV side there is a smaller relative potential between the discharge and the grounded chuck. This reduces the arc threshold and allows for proximities less than 1mm. However, it has been found that this does not increase the biofilm etching capabilities of the device. This is most likely due to the fact that the reactive ions see the grounded electrode as the preferential path despite the carrier flow gas pushing them towards the substrate.

Fig. 8 shows a disassembled single linear discharge device without an embedded ballast. The individual HV, LV and spacer plates are shown which highlights the relatively simple 3-piece construction. Pin headers are epoxied to the sides of the device, and colloidal silver paste (Ted Pella Inc. PN 16031) is applied to connect the headers to the via hole. The exposed silver spots along the trace are used to probe the ballast resistor in devices that incorporate internal ballasts. Standardization within the fabrication process allows for the choice of ballast resistor incorporation into the device without having to alter the overall design (Chapter 2 Section C).

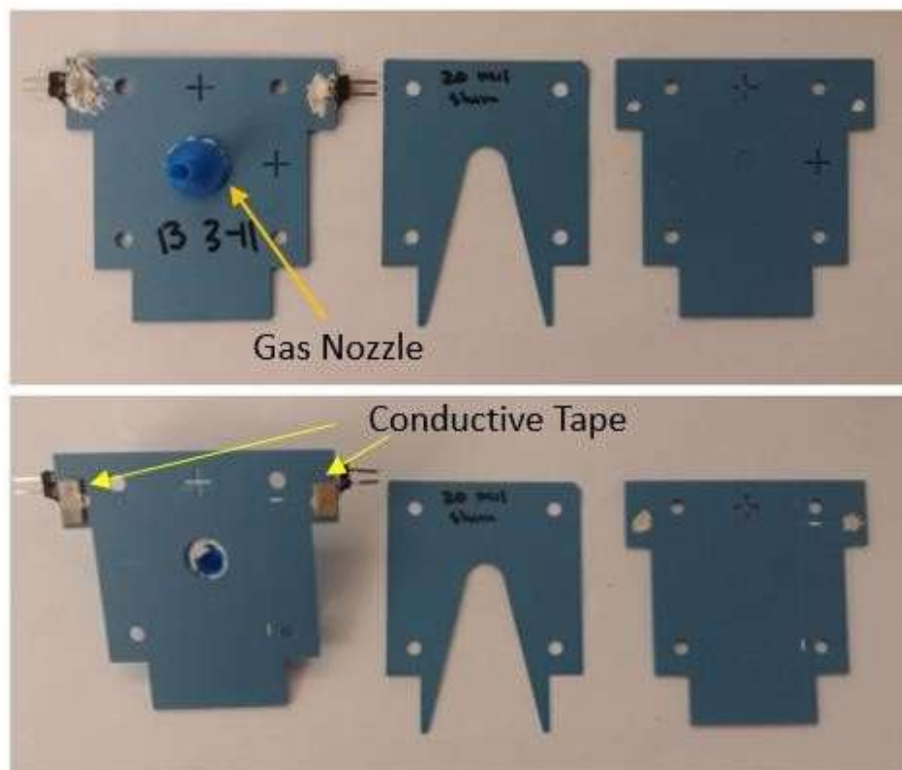

Figure 8. **(Top) Facing outwards, the 3D printed gas nozzle is epoxied to the gas porthole. (Bottom) Shown here is the inside of the device. On the front piece (bottom left), the high voltage line can be seen running down to the discharge channel. Also shown is the Double Sided Electrically Conductive Adhesive sheets by NISSHIN EM CO. LTD. The conductive sheets are used to connect the via holes together. The backside piece (bottom right) is the groundside piece and the trace is on the opposite side of the assembly to minimize capacitive coupling of the traces. The two trace pieces are separated by a 0.5 mm (20 mil) shim designed to channel the gas flow into the discharge channel.**

Multiple Discharge Array Device Overview

Multiple linear discharge devices, henceforth referred to as "arrays", have been constructed for the purpose of treating larger surface areas. Whereas single linear discharges require the substrate to be rotated below the device to completely treat the surface, plasma arrays allow larger two dimensional areas to be treated simultaneously. These devices have demonstrated success at killing bacteria biofilms (>3-log) with treatment times of 0.5-5 min. The design of the devices is similar to the single linear discharges with multiple discharges stacked together. Fig. 9 (Top) shows the front facing

view of an 8 element array. The problem of efficiently incorporating a ballast resistor with each channel has been solved by using ballast resistors built into the device as shown in Fig. 5. The dimensions of the resistor have been tailored to achieve a resistance of approximately 150 kΩ ± 15 kΩ. Fig. 9 (Bottom) shows a schematic of a three element array with parallel plasma resistance. Typical capacitance values of 8x arrays range from 12-30 pF at 20 kHz. The capacitance is approximately 8x the capacitance of a single linear discharge.

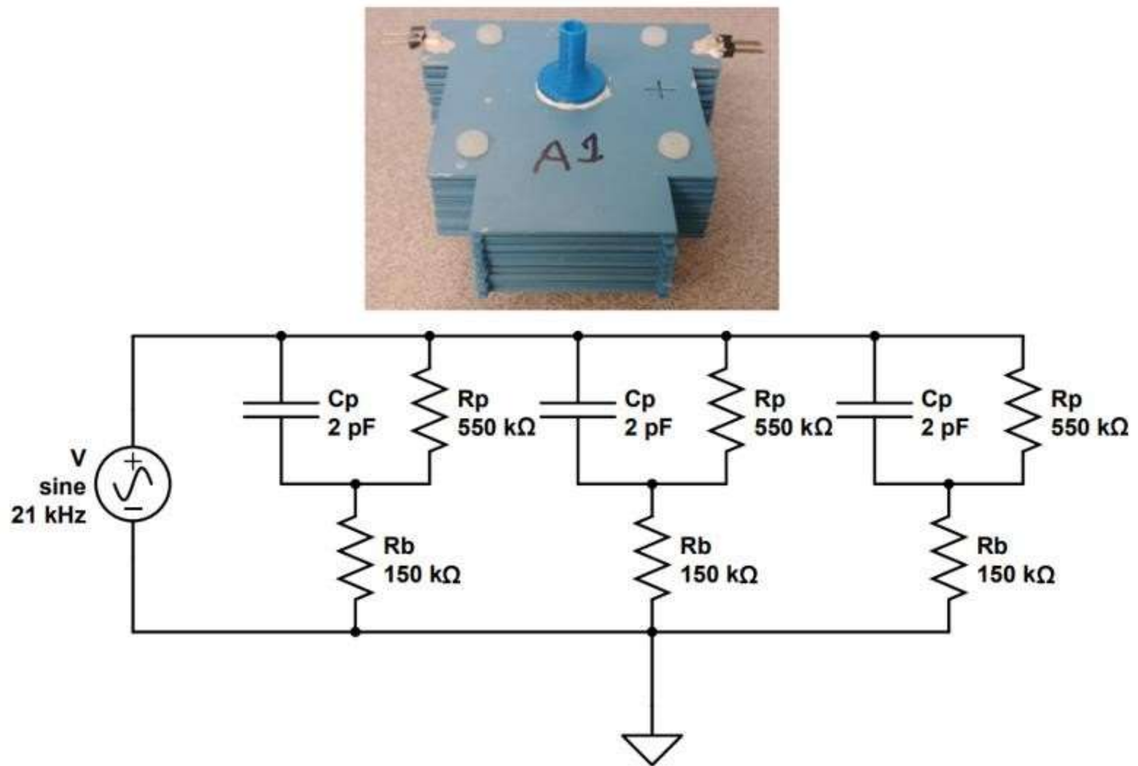

Figure 9. Top: 8 element DBD Array. The left header pin is the HV side and the right pin is the ground side. Bottom: Circuit of a 3x array. Shown here is Cp, Rp and Rb which are respectively the plasma capacitance, the plasma resistance and the ballast resistance. Additional discharges are simply stacked onto the existing assembly.

The single linear discharges are designed so that they can easily be stacked together to form arrays of discharges. From Fig. 8, the left and right header pins are electrically connected vertically to each plate through via holes and conductive tape. The first plate is a HV plate with an electrode on only one side. The next plate is a LV plate with ballast resistors built into both sides. This is shown in Fig. 5. Then follows another HV plate with electrodes on both sides. This design offers maximum modularity and is shown in greater detail in Fig. 10. It should also be noted that the diameter of the center gas hole was enlarged from 4 mm to 8.5 mm. Enlarging the gas manifold has improved uniformity in gas distribution.

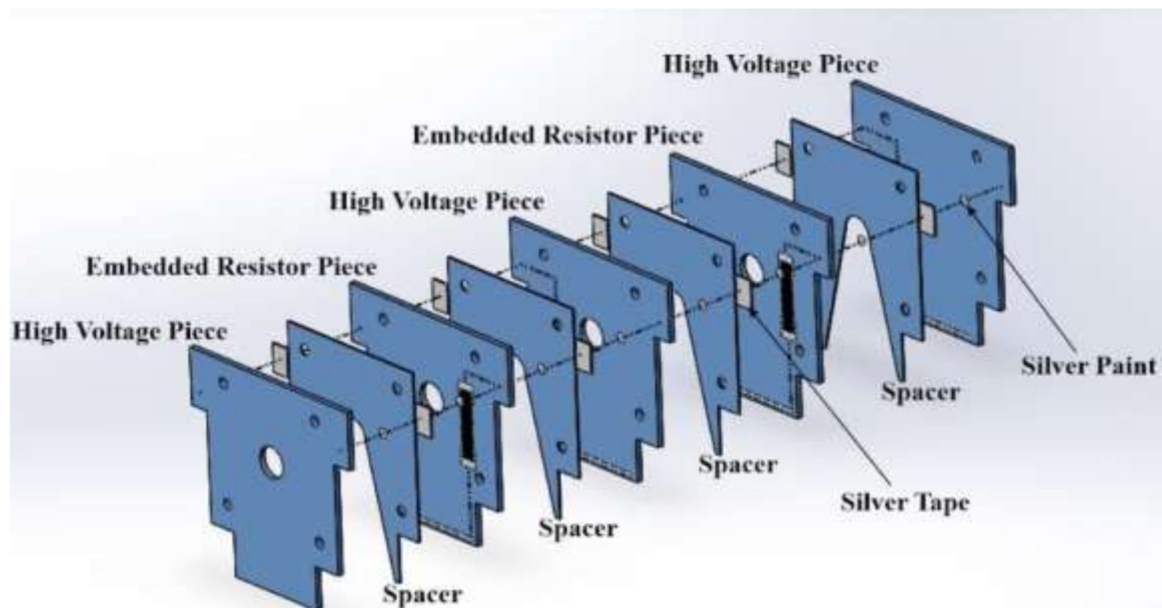

Figure 10. SOLIDWORKS Assembly of a 4x array showing how each piece from Fig. 8 is stacked together to form an array structure.

Device Design and Fabrication

The process in which the LTCC is fabricated is well documented [32,33], but it is worthwhile detailing the exact process flow of the specific devices related to this research, while noting changes made along the way for device uniformity and robustness.

First, DuPont GreenTape 951 LTCC [34] is laser cut with a Universal Systems M-300 printer to the specifications drawn using CorelDRAW12. Fig. 11 shows the CAD drawing of the individual LTCC sheets. Each LTCC sheet is 10 mils thick (0.254 mm). Increasing the thickness from 5 mils to 10 mils has dramatically reduced the tendency to form streamers in the final device. Then, thick film screens (RIV Inc.) are used to screen print silver conductor paste (903-A) onto the LTCC utilizing the fiducial marks for accuracy. The screens are 8”x10” with a mesh density of 325, wire diameter of .0009”, and .0006’’ thick at 45°. Via holes used to connect header pins to the trace on the underside of the LTCC are now filled with silver paste. The layer with the trace is then placed in a Sheldon manufacturing Inc. oven at 80℃ for 5 min.

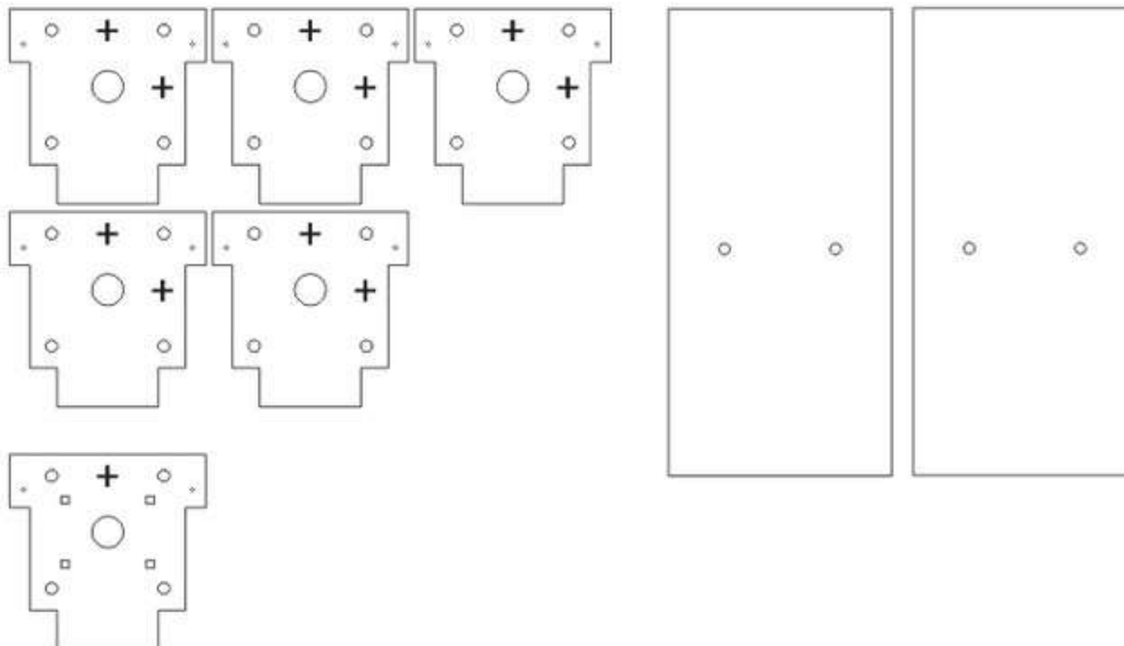

Figure 11. (Left) Five layers of 10 mil (0.254 mm) and one 5 mil layer LTCC drawn in CorelDRAW12. The + marks are fiducial holes used for alignment during fabrication. The four holes in the corners are used as screw holes for final assembly securement and mounting in the experiment setup. The center hole serves as the gas feed hole. Two 5 mil layers are used as the conductor cover sheet. This serves to protect the silver trace from oxidation during operation. The four square via holes are probe locations for measuring resistance in devices with embedded resistors. The two small holes in the corners are via holes for connecting the trace to headers mounted after final assembly. (Right) These two pieces are printed on photo paper and are used to sandwich the assembled piece in the press. The small holes are used to align the stack while being pressed. It has been found that without these pieces the assembly can stick to the press and pull apart.

Afterwards, the 10 mil sheets are assembled within the two paper press sheets and aligned with setter pins through the paper holes. The stack is set in an Agilent Thermal Lamination System model NPN, and the pressure is increased until firm to prevent cracking under higher pressure. After 10 minutes the pressure is increased to 3000 PSI for 5 min. The stack is released and rotated 180° and pressed for another 5 min. The stack is released, and the 5 mil cover layer is then covered in PEOX adhesive and mounted onto the stack. In the press, the completed stack is allowed to heat up 30 seconds and pressed for another 3 min. The stack is then placed on an aluminum setter sheet and

placed in a 1.8 kW box furnace. This is then heated via the process shown in Fig. 12. This completes the fabrication process of one side of a single discharge plasma device. The process is repeated for the opposite side of the device, and multiple stacks can be fabricated at once for increased efficiency. This procedure is repeated for the arrays for as many pieces as required. The only difference is that the LV side incorporates a ballast resistor on each side as shown in Fig. 6.

Figure 12. Furnace heat cycle for each stack of LTCC.

Improvements in LTCC design and fabrication have dramatically reduced device failure rates and increased electrical operating thresholds. Originally, a 2-mil sheet was used to cover the electrode, but it was found that the devices were more prone to failure to bright spots and pinholes. By switching to a 5-mil cover sheet, the failure rate has dropped by >90%. Generally, one wishes to cover the discharge electrode with a dielectric to increase the lifespan of the device. Without a cover sheet, the electrode would blacken and eventually fail due to the deposition of ambient organics.

Biofilm Preparation

Much of the process in producing bacterial biofilms can be found in our previous work in section *B. Biofilm Sample Preparation* [20]. However, it is worth repeating the important parameters involved in the process because the resultant biofilm thickness and profile is inherently extremely variable. The procedure is as follows:

1. Fill an empty centrifuge tube with 10 mL of Lysogeny Broth (LB) media.

2. Place 1 colony of the bacterium from the augur plate into the 10 mL of LB and shake the contents.
3. Place this tube in the shaker table at 175 rpm at 30℃ for 24 hours
4. After 23 hours, fill an empty centrifuge tube with 30 mL LB.
5. Fill a 1 mL pipette up to 0.3 mL with the culture-LB mixture.
6. Mix the 30 mL LB with the 0.3 mL culture-LB.
7. Place a substrate slide into each well of a 12 well plate.
8. Place 2 mL of the 30.3 mL mixture into each well.
9. Wrap the tray with parafilm and place in the shaker table, at the same conditions in step 3, for 48 hours.
10. After 48 hours, the samples are ready for plasma treatment.

Nonpathogenic E. coli BL-21 (ATCC 43894) and *Pseudomonas fluorescens* are the common pathogens used for this research for safety in an engineering laboratory. Fig. 13 shows a magnified image of the biofilm before plasma treatment. The majority of experiments have been conducted on *P. fluorescens* due to this bacterium's particular effluence at growing biofilms. Fig. 14 shows a typical *P. fluorescens* biofilm on steel substrate. Here it can be seen that the green colored biofilm is adhered to the surface of the stainless steel substrate.

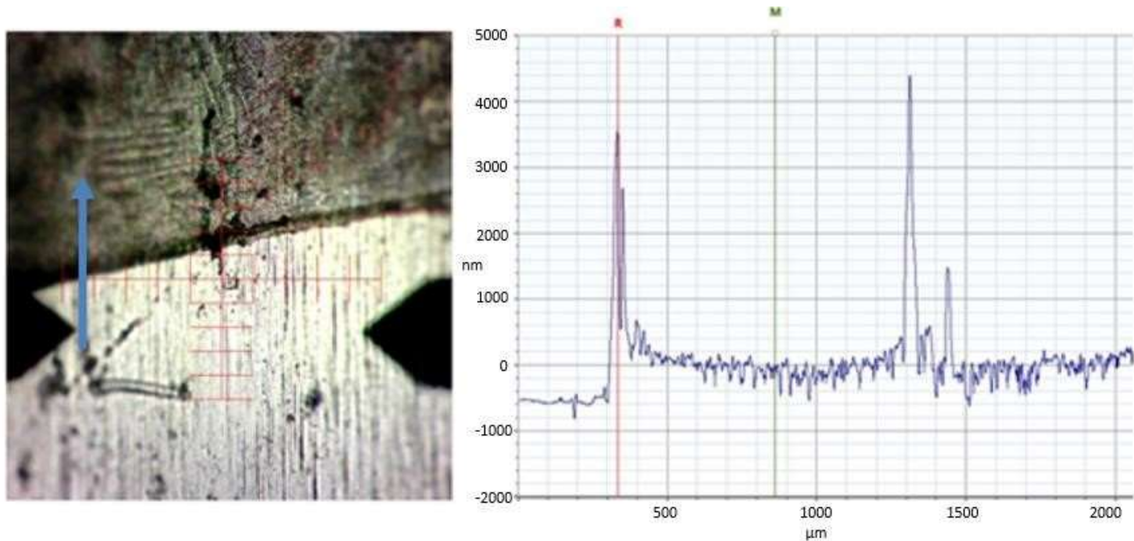

Figure 13. (Left) Image taken via Bruker Stylus Profilometer. The bottom half of the image is the steel substrate and the top half is P. fluorescens. The crosshairs indicate where the stylus (triangular shadow shown) will begin the scan. The blue arrow indicates the scan direction (Right) Shown here is the profile of the biofilm. It can be seen that the edge is the thickest part of the biofilm. This is consistent across all samples as this is where the sample submerged in LB broth meets the air. This is referred to as the oxygen boundary layer or O2 boundary. In this sample, the biofilm is about half a micron thick. This is a problem that will be addressed in Chapter 5 as it is preferred to have much thicker biofilms (≈10 µm). The negative value comes from an F operator function that helps to level the sample data.

Figure 14. Pretreatment P. fluorescens biofilm on stainless steel substrate indicated by the blue arrow. Typically P. fluorescens film thickness is on the order of 2-15 um. This image shows the biofilm after being dipped in DI water according to the experimental procedure outlined in Chapter 3.

CHAPTER 3: EXPERIMENTAL PROCEDURE

The experimental procedure is important to describe all tests involving the treatment of bacterial biofilms. This procedure picks up from Chapter 2 Section D where the process for growing the biofilms is described. All experiments in this research where etching is the objective follow this procedure.

1. Upon delivery of the samples to the engineering laboratory, the samples are either stored in a refrigerator or unwrapped for immediate use.
   a. If stored in the refrigerator (for no longer than 3 days), the samples are removed and allowed to warm to room temperature for 1 hour.
2. A sample is then removed from the broth and placed into an empty 12 well plate marked "Treated" and the date of treatment.
3. At least 2 samples are then removed from the broth, dipped in DI water 3 times and placed into adjacent wells of the 12 well plate as experimental controls.
4. All gas bottles are opened and their flow rates are set via the mass flow controllers and calibrated via the VFA-25 flowmeter. The drechsel flask and all gas lines are checked for leaks.
5. The device under test (DUT) is installed into the test stand.
6. The power supply and oscilloscope is turned on and adjusted to the frequency of the test.

7. The DUT is operated at the specific gas flow rates and voltage level determined for the test with a mirror underneath the discharge to check for bright spots and device failures.
    a. If bright spots are detected, the voltage is adjusted to beneath this threshold per that gas flow rate. This is then noted in experimental notes.
8. The mirror is removed from underneath the device and the proximity to a test substrate (without biofilm) is set via a visual scale. This is done while the device is energized to determine an arc location. If an arc occurs between discharge and substrate the proximity is increased to above this threshold or the voltage reduced depending on the experiment.
9. The device is then de-energized and gas flows shut off via on/off valves.
10. With the device parameters set, the biofilm substrate is marked to indicate where the sample is being treated. In the case of arrays no mark is required.
11. The gas flow is then turned on via the on/off valve. The device is NOT energized.
12. The marked sample is placed beneath the gas flow aligning the mark to the orientation of the discharge. This way the mark points to the section of biofilm being treated.
13. After the allotted treatment time the sample is removed and placed in the "Treated" 12 well.

14. Steps 11-13 are repeated at least 2 times for experimental gas controls. These controls determine the effect of gas flow on the sample without plasma treatment.
15. A sample is removed from the broth and placed under the gas flow. The device is energized to the voltage of the experiment for the determined treatment time.
16. The DUT is de-energized and the sample placed in the “Treated” 12 well.
17. Steps 15-16 are repeated for as many samples in the experiment.
18. All treated samples are then taken to the stylus profilometer where they are visually inspected, imaged, and scanned.
19. Profiles scans, microscope and visual images are then compiled as output data per sample.

CHAPTER 4: DEVICE CHARACTERIZATION

Characterization of DBD Single Linear Discharge Devices

Electrical operating parameters are necessary for the determination of the treatment levels in future experiments. Prior work has shown that the inclusion of a ballast resistance in series with the capacitive discharge improves the uniformity of the plasma. This is useful when creating arrays of parallel devices where the possibility of having a less than optimal discharge current is increased. The ballast resistor brings the operating current of each channel closer to one another so that one channel does not become too intense before the others have initiated. This method improves the uniformity of the discharges in multi-channel arrays. This is useful even in single channel devices such that the discharge is more easily controlled, and the intensity of potential bright spots is reduced. It has been experimentally determined that 100-150 kΩ is a satisfactory ballast resistance for generating uniform discharges in the region of 3-5 kV. The current transformer shown in Fig. 3 allows for easy measurement of the current through the discharge and calculation of associated voltage drop across the ballast resistor.

Argon gas flow has been determined to be a significant component in plasma formation and intensity due to its high ionization cross section. It is necessary to determine how the gas flow interacts with the plasma in the devices used in this research. Fig. 15 shows the visual difference between an argon plasma in a single linear discharge device and an ambient air plasma. Fig. 16 shows that specific regions of the discharge can be argon based or air based within the same device.

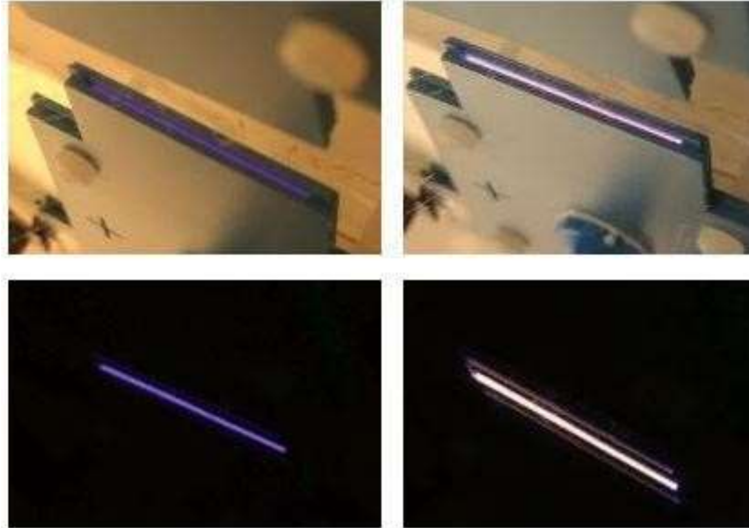

Figure 15. Photograph of a single linear discharge CAP device with and without gas flow. (Left) No Ar gas flow (Ambient air) at 2 kV. (Right) 5 LPM Ar gas flow at 900 V. Notice the stability and uniformity of the discharge.

Fig. 17 shows the difference in IV characteristics of an argon plasma vs ambient air plasma. The linear fit equations are displayed and are used for calculating an equivalent resistance of the DUT.

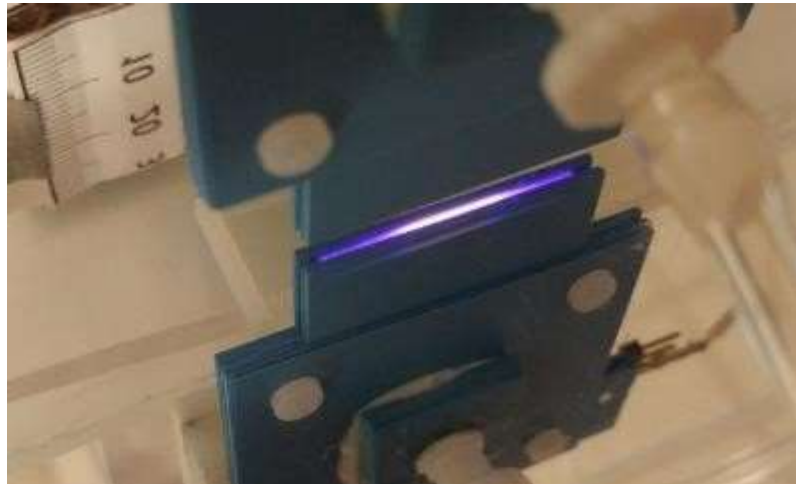

Figure 16. Photograph of multi-gas discharge operating at 2 kV with 5 LPM Ar flow through the center of the discharge with ambient air discharges on the edges. Note the stability of the discharge even when under multiple gas flow conditions.

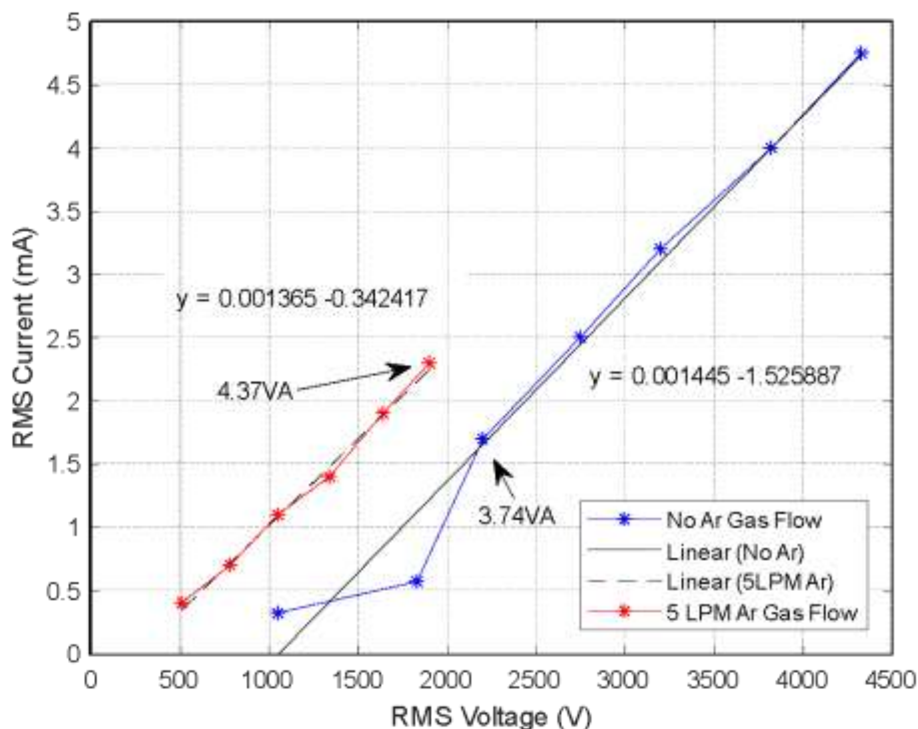

Figure 17. The red trace is the IV of a single linear discharge device with 5 LPM Ar gas flow. In blue is the IV when no Ar gas is flowing through the device. The line fits are used to determine the equivalent resistance of the device while operating.

It is worth noting that <10% of the applied voltage is wasted across the ballast. The jump in Fig. 17 at around 1800 Vrms is when the plasma begins to initiate. Initially, it is a nonuniform discharge as shown in Fig. 1, but when the slope levels out (in this case around 2200 Vrms) the plasma has reached visual uniformity and is stable. Visual uniformity is the metric used for determining the lower limit of the plasma operating region.

From Fig. 17, the slopes of the two curves are nearly identical yielding a system equivalent resistance (R_{eq}) of approximately 700 kΩ for both cases. The two points with apparent power values labeled correspond to the same knob position on the power supply. Thus, the power supply is coupling more efficiently to the discharge when argon is flowing. Also apparent is the almost immediate transition into a stable discharge ≈500

Vrms. The two points in Fig. 17 with power values marked are taken at the same voltage knob position. Thus, when argon is flowing, there is a 0.63 VA increase in apparent power delivered to the plasma per the same output position. With the increased current, the voltage across the ballast increases, further reducing the “Turn on” voltage of the argon plasma. This is expected, as the ionization cross section is much higher for argon than for ambient air.

With the improved coupling to the argon plasma, it must be determined whether or not system resonant frequency has shifted within the range of our power supply (20-70 kHz). Shown in Fig. 18 is the RMS voltage magnitude response vs frequency for argon plasma at 5 LPM vs ambient air plasma.

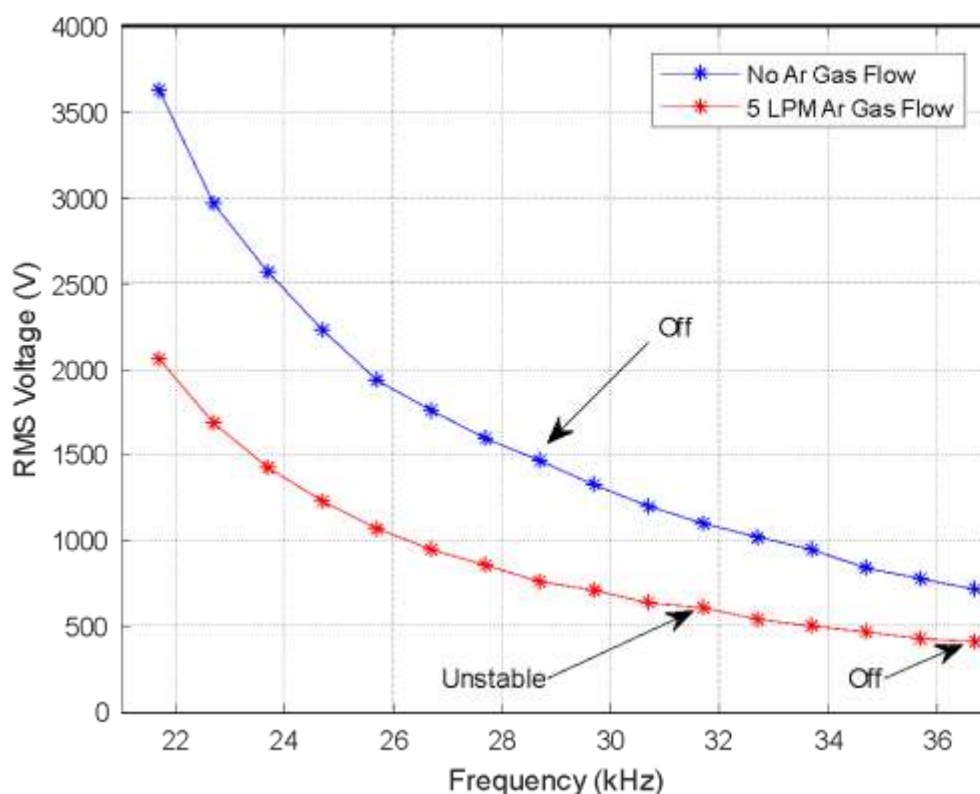

Figure 18. Magnitude Vrms vs frequency for 5 LPM Ar flow and 0 LPM (Ambient air). The starting points were selected based on the upper threshold for safely operating the device. At voltages >2 kVrms with Ar flow, the discharge begins audible cracking due to the intensity. Gap width =20 mil (0.508 mm).

It is worth noting that the ambient air discharge turns off at 1470 V (28.7 kHz); whereas the argon plasma becomes unstable at 550 V (31.7 kHz) and is definitively off at 412 V (36.7 kHz). The frequencies of instability/off will shift with a larger starting voltage magnitude. To clarify, if the sweep had begun at 5000 V at 21.7 kHz with no argon flow, the plasma "Off" frequency would be greater than 21.7 kHz but the voltage magnitude would be the same. It is the voltage magnitude that determines the actual state of the plasma. Fig. 18 serves to show the general magnitude response of the system. It also shows that argon plasmas have a much wider operating frequency range when compared to atmospheric air. The specific band is dependent on device gap width and

|Vrms| at the starting frequency. The definitive benefit of argon plasma is the reduction in required excitation voltage, improved power delivery to the plasma, and improved operating range. Fig. 18 shows that the ratio between the turn on voltage and off voltage is 40% for no argon flow and 37% for 5 LPM argon flow. This suggests that the argon has slightly lowered the percent magnitude loss per frequency, which further supports the increase in operating bandwidth. From this data, it is impossible to tell if the resonant frequency has shifted due to the resonant peak being lower than the power supply's minimum frequency.

Fig. 19 shows the effects of the argon and air discharges on the voltage and current waveforms. The current waveforms in each picture have distortion and noise due to the plasma. Interestingly, the left graph has a sharp rise in current every 180° that is relatively noiseless when compared to the noisy transition when Ar gas is flowing. It can also be seen that the currents' phase advance is approximately equivalent in both cases. This demonstrates and confirms that the argon gas does not shift the inherent resonant frequency by altering the impedance of the system.

The previous IV curves have been unidirectional sweeps for determining general operating conditions. It is, however, interesting to see bidirectional sweeps as shown in Fig. 20 and Fig. 21. It can clearly be seen that the ambient air plasma maintains sustainability over a larger decrease in voltage than the argon plasma. The air plasma maintains stability over a 400 V drop while the argon plasma turns off much quicker. This can also be seen in the frequency response from Fig. 18.

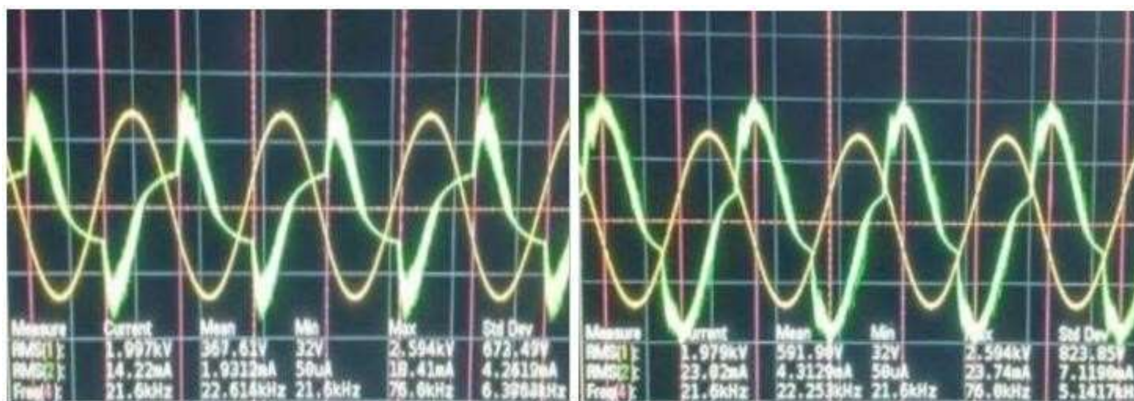

Figure 19. Corresponding current and voltage waveforms for Fig. 17. (Left) No argon flow. (Right) 5 LPM argon flow. The current readings are 10x higher than actual because the Agilent DSO5014A oscilloscope did not have a 50 V/A setting Therefore a reading of 23.02 mA actually is 2.302 mA. Note the current waveform shows the distortion from the plasma.

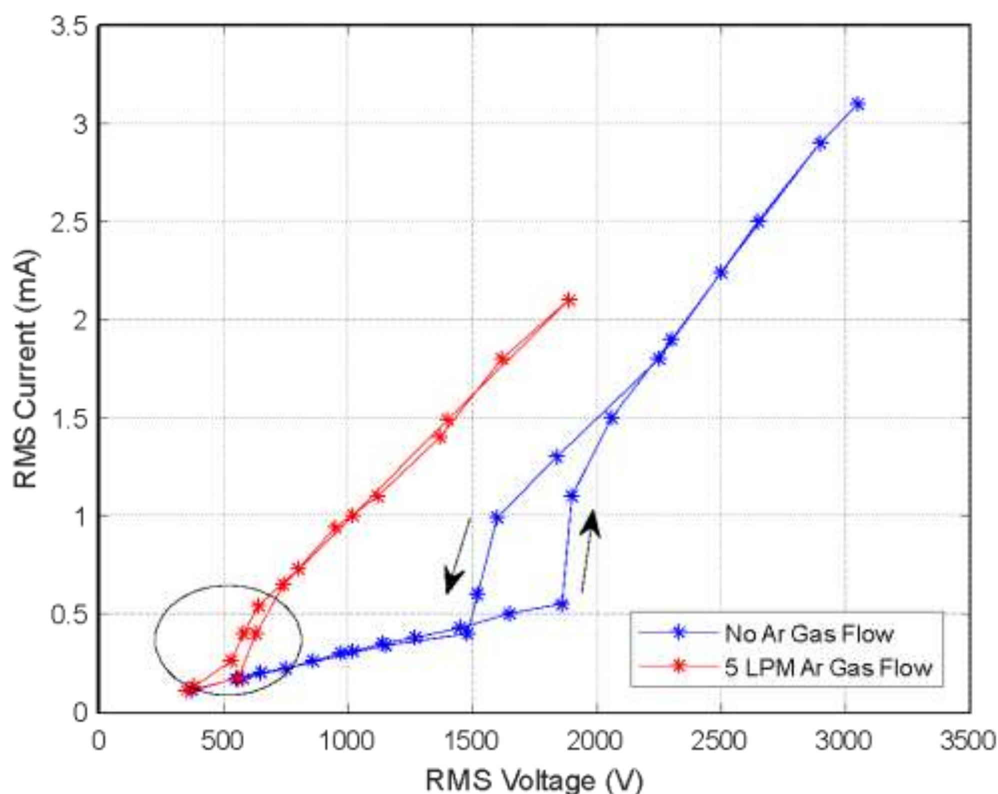

Figure 20. Current vs voltage plots of Argon gas flow and no gas flow. The circled section is magnified and shown in Fig. 21. The arrows indicate which direction the voltage is changing i.e. increasing then decreasing.

Though the argon plasma turns on much easier at lower voltages, it operates over a more narrow range of magnitudes, and the device can fail at lower voltages when compared to air plasmas. Fig. 20 and Fig. 21 clearly demonstrate that the area enclosed by the argon gas discharge curve is much smaller than the area enclosed by the air discharge. This difference in hysteresis is expected due to the fact that oxygen and nitrogen atoms require greater energy to ionize. When de-excitation occurs, the ions release more energy than a negative argon ion returning to ground state. Thus, it is expected that oxygen plasmas have a greater thermal signature when compared to argon plasmas at equivalent power densities and flow rates.

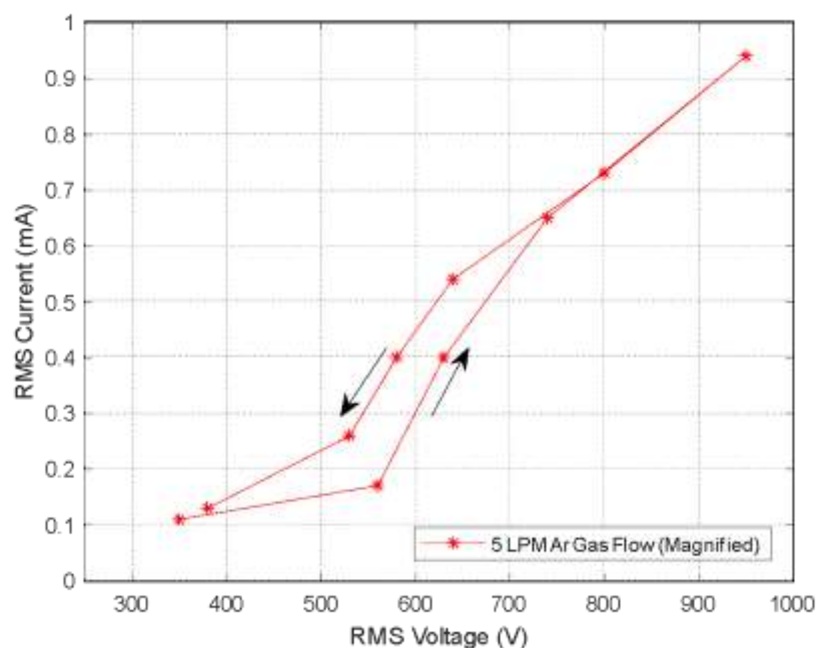

Figure 21. Magnified current vs voltage plot of 5 LPM Ar flow.

An important consideration for NTP is the temperature at the electrode and thermal profile of the substrate over time. The upper thermal threshold is around 35°C for biofilms. At this point, thermal processes begin killing the bacterial biofilm, and these effects cannot be distinguished from other plasma processes. Thermal measurements via

a FLIR systems ThermoVision A320 Camera have shown that a single linear discharge device at 2 kV with 5 LPM increased the substrate temperature from 3℃ to 27℃ as seen in Fig. 22. At this treatment combination 2.3 mA was generated through the discharge. Even at 1 mm to the substrate after 5 minutes the temperature of the steel has only increased by 1℃. It should be noted that all thermograms shown share a similar object of interest. In Fig. 22 the white arrow points to the edge of the steel substrate. At the edge, the infrared reflection of the plasma discharge is superimposed onto the infrared generated by the substrate due to heating from the discharge. This is because the emissivity of the substrate allows IR to be reflected. The back half of the substrate reflects IR as well, but due to the angle of incidence upon the substrate it is not picked up by the IR camera. This gives an approximate temperature of the discharge itself by subtracting the temperature in the area of generation from temperature in the area of generation and reflection.

Figure 22. Thermogram of single linear discharge plasma device operating at 5 LPM Ar flow, 2 kV and 2.3 mA after five minutes of exposure. The gap between the electrodes is 1.2 mm and the device is 3 mm above the substrate. The temperature range shows the maximum and minimum temperature in the image to be 29.4℃ and 23.6℃ respectively. The steel heats only to 25℃ which is far below the 35℃ threshold.

The scale on the right of the thermogram is the range of temperatures present in the image with the top left being the temperature within the crosshairs. Experiments have shown that substrate heating is not a concern for the single discharge devices under all operating regimes. It is, however, a concern for the arrays and will be presented in Chapter 4 Section B.

Arcing from the discharge to the substrate is a constraint on all operating regimes. It is easy to see that this is a function of proximity and voltage. For many of the experiments shown in Chapter 5, the device is operating just below this threshold. These devices are capable of functioning while arcing for a few minutes before device failure. The arcing regime is not conducive to device longevity, regardless of its effect on bacterial biofilms. Fig. 23 shows typical arcs seen with single linear discharge devices.

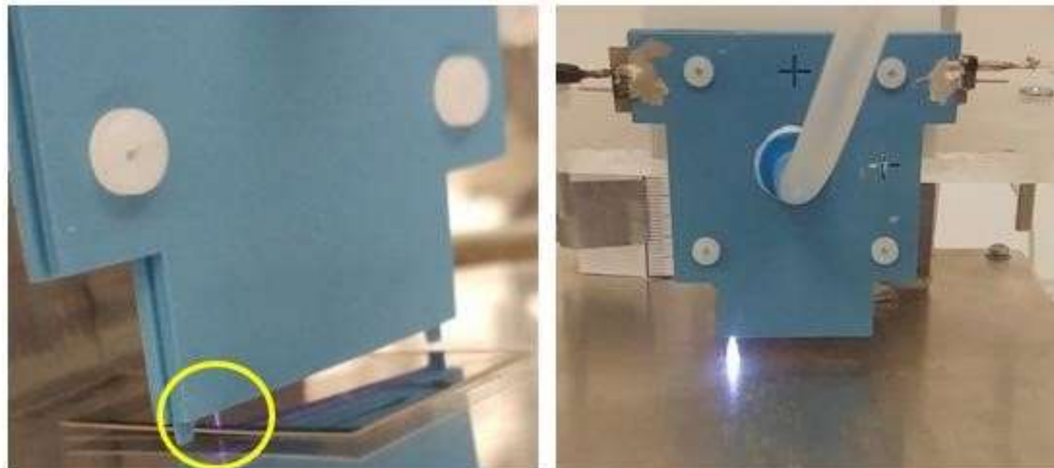

Figure 23. Photographs of typical arcs from a single linear discharge device. (Left) Treatment settings: 1.6 kV, 1.2 mm gap, 1 mm to substrate, 5 LPM Ar, external ballast 100 kΩ. A small arc to substrate is shown circled. (Right) 4 kV, 1.2 mm gap, 5 mm to substrate, 5 LPM Ar. These are typical arcs seen when the discharge channel is brought too close to the treatment surface or ground chuck.

Characterization of DBD Multiple Discharge Plasma Arrays

Similar to single linear discharges, it is necessary to see the electrical response and IV characteristics of the array devices. It is expected that these devices respond similarly to the single linear discharges, while anticipating a few notable differences. It is anticipated that these devices will see a small amount of capacitive coupling between channels. Also, gas flow per discharge should be relatively small compared to the total flow rate. This introduces a few problems such as discharge intensity per channel and convective heating of the substrate. These will be addressed in this section. Fig. 24 shows an 8x internal ballast resistor array operating under standard operating conditions.

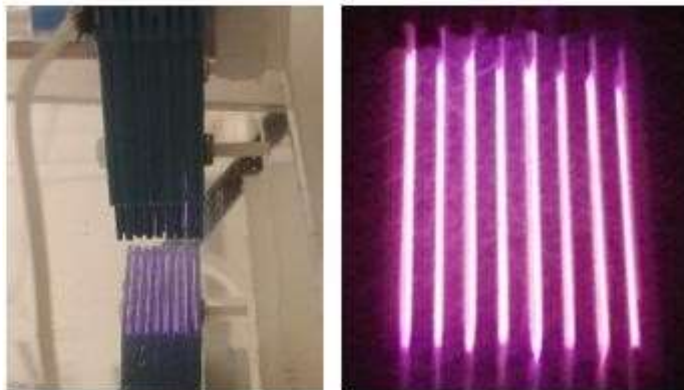

Figure 24. Photograph of an 8 element internal ballast resistor array 'A1' from Fig. 8 operating at 900 V, 9.5 mA with 9 LPM Ar flow.

By using a test array such as the one shown in Fig. 24, each channel can be selectively excited. This is accomplished by removing the conductive via connection between each discharge. This requires each channel to have its own HV and LV wire. Each channel is then connected to its own external ballast resistor. It has been found that each channel is effectively isolated from one another up to 4.5 kV. External ballast resistors are used to perform IV sweeps on each channel so that the impact of different ballast resistors, as well as the impact of capacitive coupling can be seen.

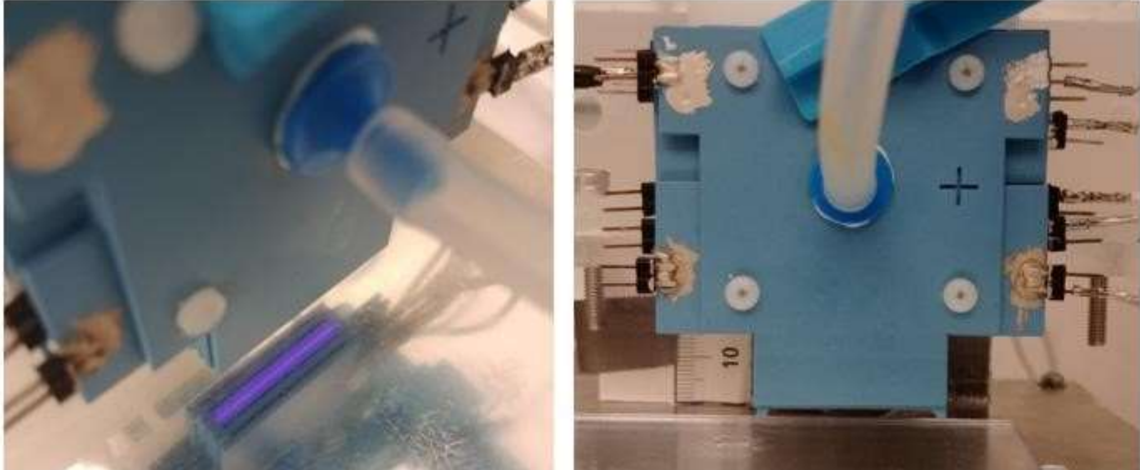

Figure 25. Photograph of a test array with isolated channels. (Right) A five channel array constructed so that each discharge channel is isolated from one another. This allows for independent channel selection and IV characteristics in situ. (Left) The center discharge of the test array operating at 4 kV without gas flow with 100 kΩ ballast.

First, IV sweeps were conducted on each independent channel of the 5x array. This means that only one HV line was connected and one LV line was connected to an external ballast. Thus, the excited channel would only see a minimal amount of coupling, if any, to the other 4 channels. Fig. 26 shows the results of the sweep per channel at various ballast resistances. Fig. 27 is an averaged IV per ballast resistance from Fig. 26.

The 1 kΩ IV curve, whose current rises much faster than the others (indicated by the black arrow pointing down), was due to a bright spot beginning to form. Increasing the ballast resistance helps to fix potential failure points like these by dropping more voltage across the resistance instead of across the discharge. It also reduces the channel to channel variation, thus improving uniformity.

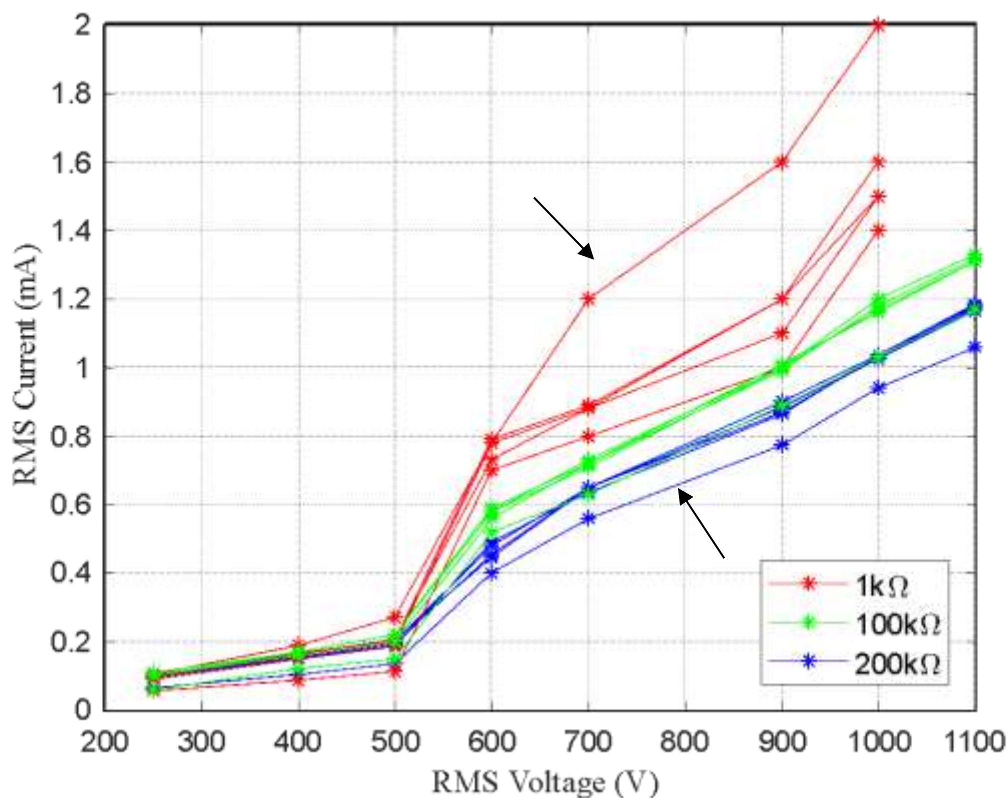

Figure 26. IV data for 1 kΩ, 100 kΩ and 200 kΩ external ballast resistors with 5 LPM Ar flow gas. The 1 kΩ data lacks an 1100 V data point due to significant channel to channel arcing beginning to occur. The arrow pointing down indicates an element that developed a bright spot. The arrow point up indicates an element that exhibited a fabrication defect.

Immediately, it can be seen that with a 1 kΩ ballast, the current begins to increase rapidly after 900 V. Further data was not collected for 1 kΩ as arcing began to occur. This highlights one the most important aspects of the ballast: extending the operating range and uniformity of the device. The channel indicated by the black arrow pointing upwards can be seen to be outside the grouping of the other four discharges for both 100 kΩ and 200 kΩ ballasts. This can be due to a number of reasons including misalignment of the electrodes or an error in the fabrication process, but in this case the channel was replaced entirely and a cause could not be tracked down. It would not be possible to test each channel independently in devices with built in ballast resistances. It has generally

been seen that channel currents can swing within 10% of each other without detrimental effects in these devices.

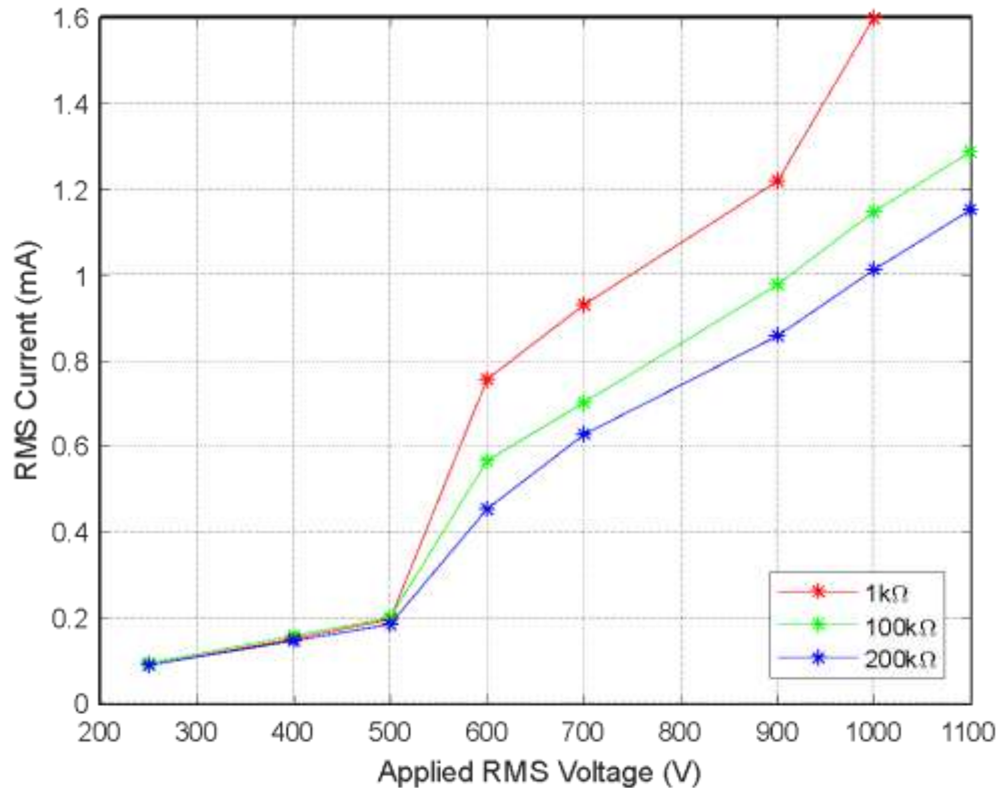

Figure 27. Averaged data points from Fig. 26. This is a cleaner visualization of the effects of the external ballast resistor.

From Fig. 26 and Fig. 27, it is clear that 100 kΩ significantly improves the uniformity and operating range while increasing the required voltage to turn on. A 200 kΩ ballast increases this further without much improvement in uniformity. Given the stability of the two ballast resistances, 150 kΩ is a logical compromise of uniformity between robustness to arcing and turn on voltage. With variability in the ballast resistor fabrication process of approximately ± 10%, this resistance value gives a comfortable margin for channel uniformity, stability and confidence for deployment in multi discharge devices.

The coupling between channels is of interest in the arrays. This coupling can influence device equivalent resistance, resonance and arc thresholds. Fig. 28 demonstrates the effect of coupling on a 5x array. This experiment demonstrates the channel to channel capacitive coupling. It is performed with 1 HV line coming into channel one and all channels ground sides connected to external ballast resistors.

Though this is not how the device will operate under normal conditions, it does serve to show that there is this coupling between channels at normal operating voltages. This may or may not be a problem for tuning a resonant circuit to the arrays which will be briefly discussed at the end of this section.

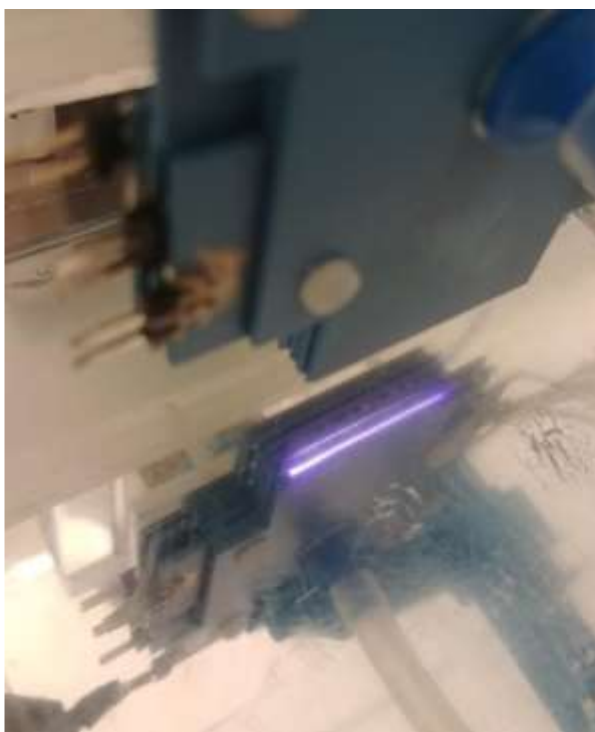

Figure 28. Photograph of a single HV line igniting a weaker stable plasma in the second channel and a transient plasma in the third via capacitive coupling. Since each channel is electrically isolated, it is the capacitance of the LTCC that the voltage on channel 1 is coupling through. This occurs at >3.5 kV for this device with 5 LPM of Ar flow.

An IV sweep of the test device in Fig. 25 is shown in Fig. 29. The red trace represents when the channels are electrically isolated by leaving the other channels floating. The blue trace is coupled because one HV line excites a discharge in an adjacent channel with all channel's ground sides connected to individual ballast resistors. This allows each channel to see a capacitively coupled AC signal of varying magnitude based on proximity to the primary channel. When the channels are coupled, there is clearly an increase in displacement current before the plasma has turned on. It is also apparent that the equivalent resistance R_{eq} of the device has decreased with the additional coupling. This is clear from the inverse relationship between increasing parallel capacitance and total impedance.

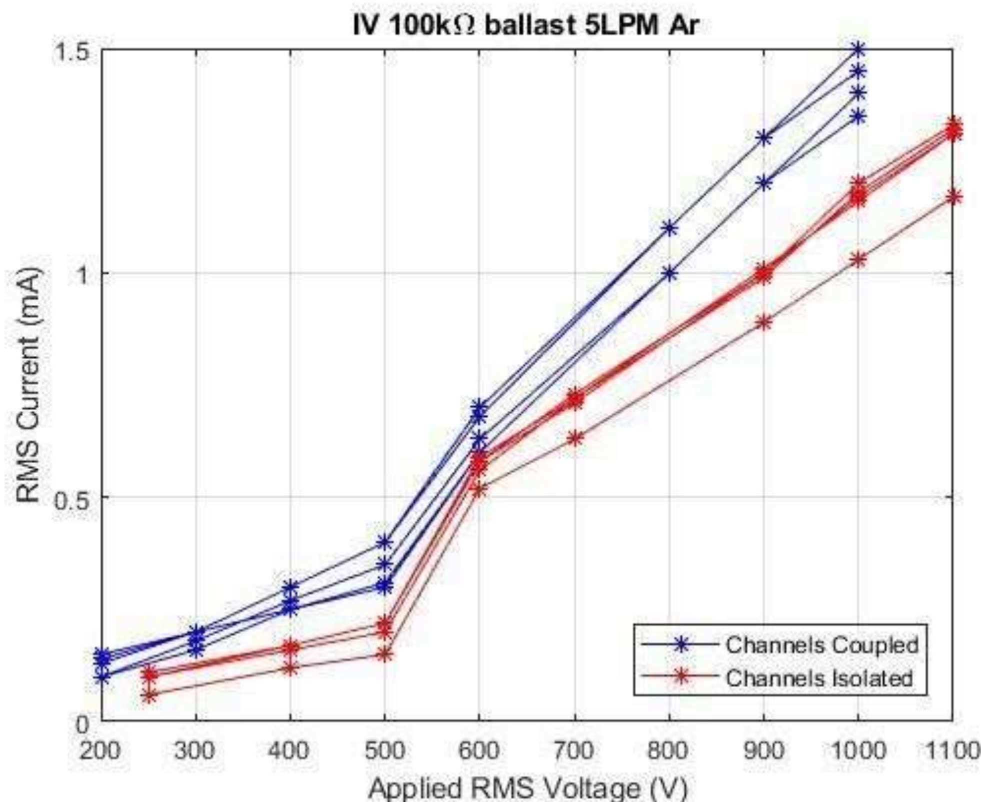

Figure 29. IV comparison between coupled and isolated channels, both with 100 kΩ ballast resistors. Clearly there is a difference in behavior between multi-discharge arrays and single discharge devices in an array configuration. This represents a drop in equivalent resistance from 750 kΩ to 440 kΩ.

Thermal effects are a significant consideration for the array devices. For an 8x array operating at 1500 Vrms and 10-12 mArms has a minimum 15 VA delivered to the device. This constitutes significant local heating. Thermal analysis of the device is necessary for ensuring that the bacterial biofilms remain below the thermal kill threshold of ≈ 35 - 37℃. Fig. 29 shows a thermogram of an 8x array over a 5 minute period. For the following thermograms, the substrate is sitting within a small petri dish. The gas flow rates are adjusted in order to determine the effect of flowrate on substrate temperature at 2mm proximity. It is necessary that the arrays operate well within the thermal thresholds. Otherwise, the effects of the plasma processes would be confused with thermal processes.

Fig. 30 shows that with no gas flow the substrate temperature is noticeably increased from 29.1°C to 32.5°C when compared to the single discharge. This is determined by the spot value in the upper left of each figure. This constitutes a 7.5°C increase above the single linear discharge shown in Fig. 22. Fig. 31 shows the effect of flowing 6 LPM of argon gas through an 8x array.

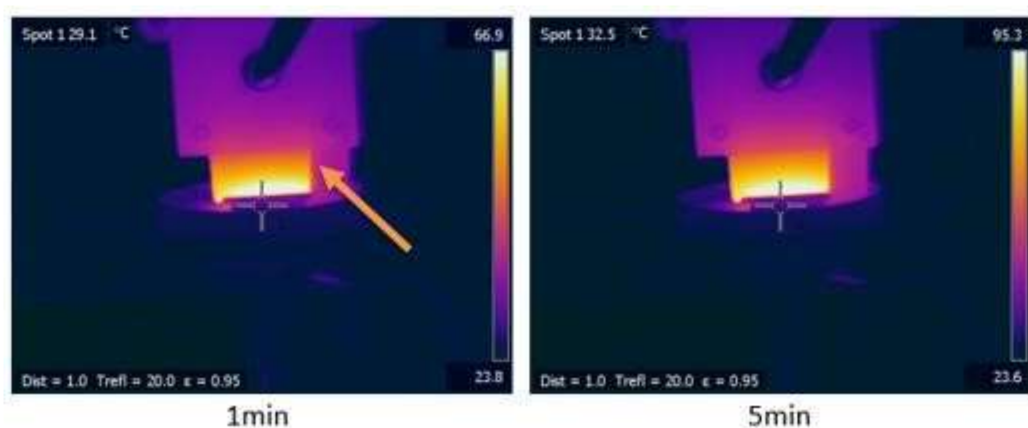

Figure 30. Thermogram over time for an 8x Array operating at 2 kv with 9 mA and no flow gas. The orange arrow points to a small LTCC piece attached to the device that sets the proximity to the substrate. After 5 minutes the substrate remains safely below the thermal kill threshold.

From Fig. 31, it is clear that additional convection is required to keep the substrate below the thermal kill threshold. Fig. 32 shows the effects of increasing the flow rate to 13 LPM Ar. This flow rate keeps the steel substrate well below the thermal threshold. It must be noted that although the prior hysteresis plots suggest that air plasmas will be hotter than argon plasmas, it is clearly not the case for Fig. 30-32. This is because these tests were conducted at operating point extremes. Thus, an argon plasma running at 2 kV is much hotter than an oxygen/atmosphere plasma at 2 kV.

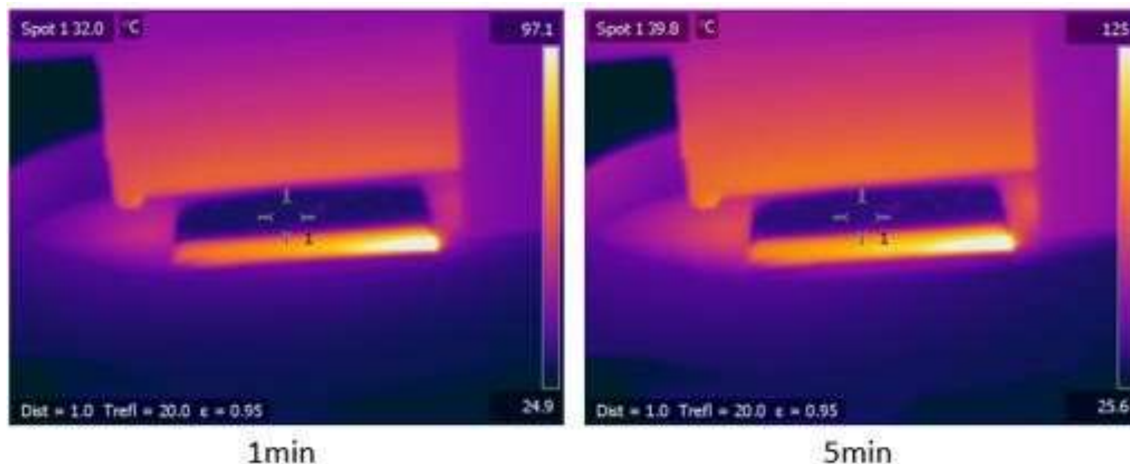

Figure 31. Thermogram of 8x Array at 2 kV after 5 minutes with 6 LPM Ar. From the spot measurements, it is clear that the plasma is much more intense (39.8℃) than that of Fig. 30 (32.5℃) where no gas was flowed. Though more convective heat transfer is taking place via gas flow, the intensity of the plasma causes the substrate to heat up beyond the thermal kill threshold. The amount of heat removed from the substrate via gas flow is unable to keep up with the rate of heat delivered.

One observation from these thermal measurements is that lower argon flow rates heat the substrate faster than no gas flow at equivalent voltages. This is due to argon plasmas being much more intense and dissipating more heat through the plasma resistance, compared to ambient air based plasmas at the same voltage. Clearly, higher flow rates are needed to keep the device below the thermal kill threshold. The effect of other flow gas media was not tested as argon gas is good for achieving intense plasmas while considering the cost of other noble gases with even higher ionization cross sections.

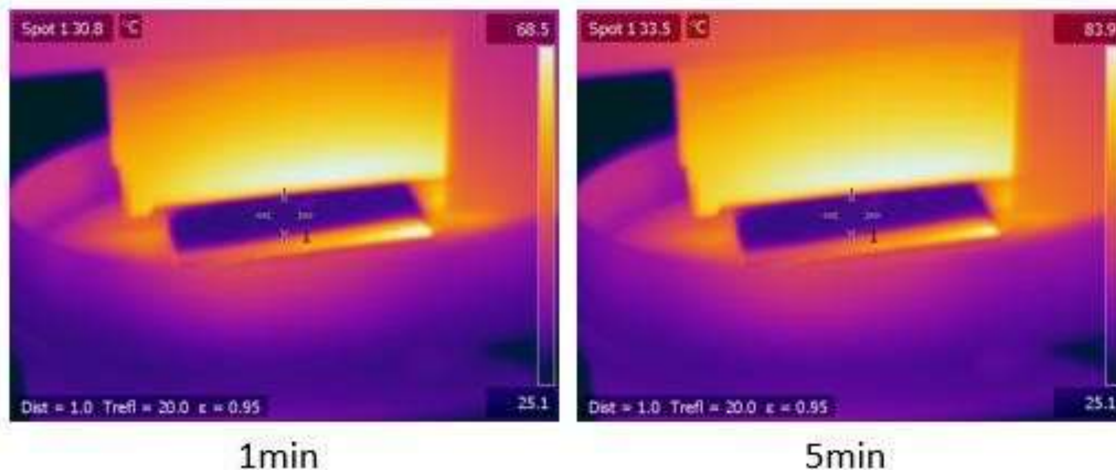

Figure 32. Thermogram of 8x array at the operating conditions outlined in Fig. 31 except with 13 LPM of Argon gas flow. After 5 minutes the substrate is well below the kill threshold at 33.5°C. It can also be seen the device itself remains much cooler throughout the treatment cycle via the max reading on the right side of the figure.

One concern with large arrays is the power draw and efficiency of the devices. The PVM 500 power supply is limited to a frequency range 20 kHz- 60 kHz. Thus, it is believed that by introducing a parallel inductance, a resonance effect can be created between the inductor and the capacitance of the DBD. It is expected that there will be one resonant frequency pre-ignition due to the circuit reactance, and another when all elements have turned on. This would be due to the capacitive nature of the plasma during operation. From the resonant frequency equation of an RLC circuit if the capacitance increases, the resonant frequency should drop. The standard operation of an 8x array versus that of when a parallel inductance is introduced is important for determining any adverse effects the inductance may have. Array device A1 as depicted in Fig. 8 is used and a rough schematic is shown in Fig. 33.

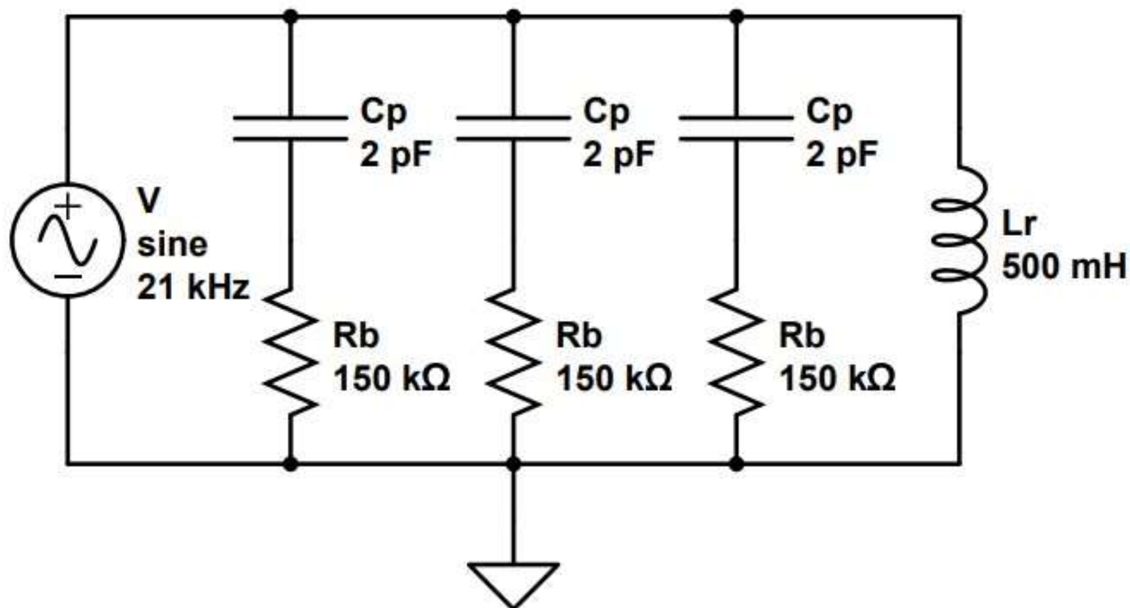

Figure 33. Schematic of a 3x array with parallel inductance Lr.

By using a parallel inductance of ≈ 500 mH a resonant peak is achieved around 33 kHz. Fig. 34 shows the voltage and current waveforms pre-ignition. Fig. 35 shows the waveform at resonance after adjusting for the plasma on capacitance. It can be seen that the current in the pre-ignition state leads the voltage by about 10 us/div. This equates to a phase shift of 80° and a power factor of 0.17. This is clearly not the most optimal power delivery system, but it does create a resonant peak within the range of the available power supply. Compared to Fig. 20 where the current lags the voltage, this circuit is now capacitive as the parallel inductance tuned out the power supply's high voltage transformer.

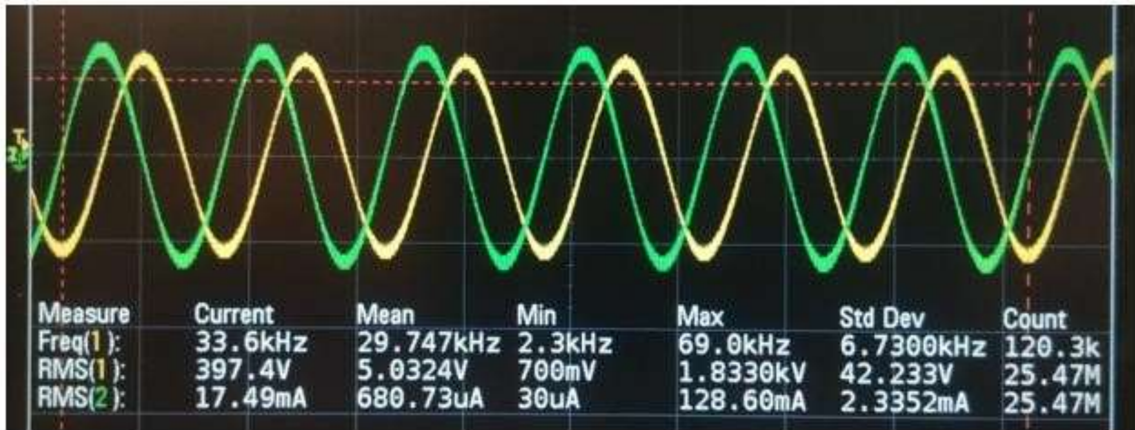

Figure 34. Pre-ignition waveform with parallel inductance. 33.6 kHz is the resonant peak. Note that the current is 0.1x RMS(2) = 1.7 mA.

Interestingly, there is not an increase in the power supply's ability to deliver power with the addition of the parallel inductance. Nor is there an increase in current through the device. There are two significant effects the inductance has introduced. The first is a shift in resonant frequency. The second is that all channels in the device turn on almost simultaneously without any visible transient phase, at the same turn on voltage. Compared to standard operation without a resonant inductance, each channel has a gradual turn on as the voltage increases. This may or may not be a necessary quality as in practice, the device would operate in saturation via a TTL input to the power supply. The voltage setting would be preselected and no manual ramp up would be necessary.

Figure 35. Current and Voltage waveforms of an 8x array with resonant inductance. Similar to Fig. 19, there is similar distortion on the current waveform. However, the noticeable difference is that in Fig. 19 the noise occurred after the peak of the sinusoid. Whereas with the resonant inductor the noise occurs pre-peak. The new operating resonant frequency is 25.5 kHz as shown.

Arrays demonstrate similar arcing behavior as single linear discharge devices. Experiments in Chapter 5 were designed to ensure that arcing does not take place between discharge and substrate. This means that as voltage and proximity are adjusted until arcing occurs, then one or both parameters are adjusted to remove the arc. Fig. 36 shows a typical arc from an 8x array and demonstrates how critical it is to maintain the device below the arc threshold.

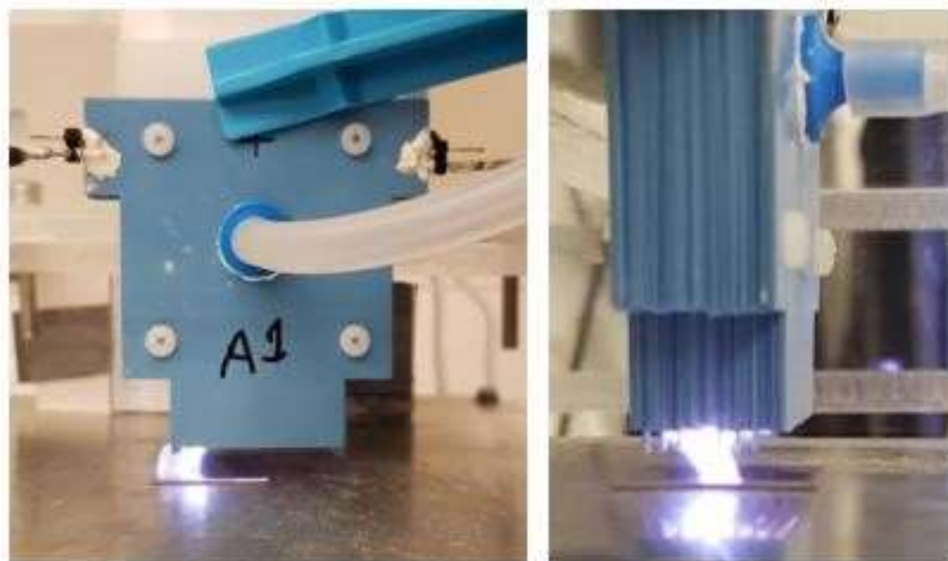

Figure 36. A typical arc generated from an 8x array to a grounded substrate. This particular device arcs at 1500 V at 4 mm to the substrate with 5 LPM Ar.

CHAPTER 5: CAP TREATMENT OF BACTERIAL BIOFILMS

Overview

The purpose of single linear discharge and array devices is to kill and remove bacteria from substrates relevant to the food processing and medical industries. This chapter presents an overview of the effectiveness of the devices at killing bacteria. It also presents a culmination of the work done in order to achieve etching of the biofilms via plasma processes. Though further testing and optimization is necessary, there is preliminary etching at specific treatment combinations. The variable nature of these biofilms introduces significant inconsistency into the experimental process. Though etching for one batch of samples at specific treatment combinations may occur, it may not with the next batch. Much of the analysis was performed via images and scans taken with a Bruker Stylus Profilometer. For the purpose of the discussion, a few case studies will be selected and the results analyzed.

Previous results have shown that single linear discharges are capable and effective at inactivating bacterial biofilms. Using the process outlined in Chapter 3, many experiments have been performed relating to the efficacy of the devices on multiple substrates with various organisms. Substrates include glass, plastic, rubber, 430 2BA stainless steel, and porcine tissue. Fig. 37 shows various bacterial CFU counts over 60 seconds on stainless steel. Clearly, it can be seen that the plasma treatment has a significant impact on the total remaining colonies. It has been found that in some cases, the inability to reach >3-log reduction has been due to partial contamination from the sides of the substrates. By not cleaning the substrates edges, i.e. area not under plasma

treatment, it can artificially inflate the CFU counts and lead to a reduction in perceived efficacy. It was calculated that this can introduce as much as 15% additional CFU's. This was fixed by using an updated procedure process, and these results will be presented in future papers. It is, however, obvious that even with this error, there are considerable reduction capabilities.

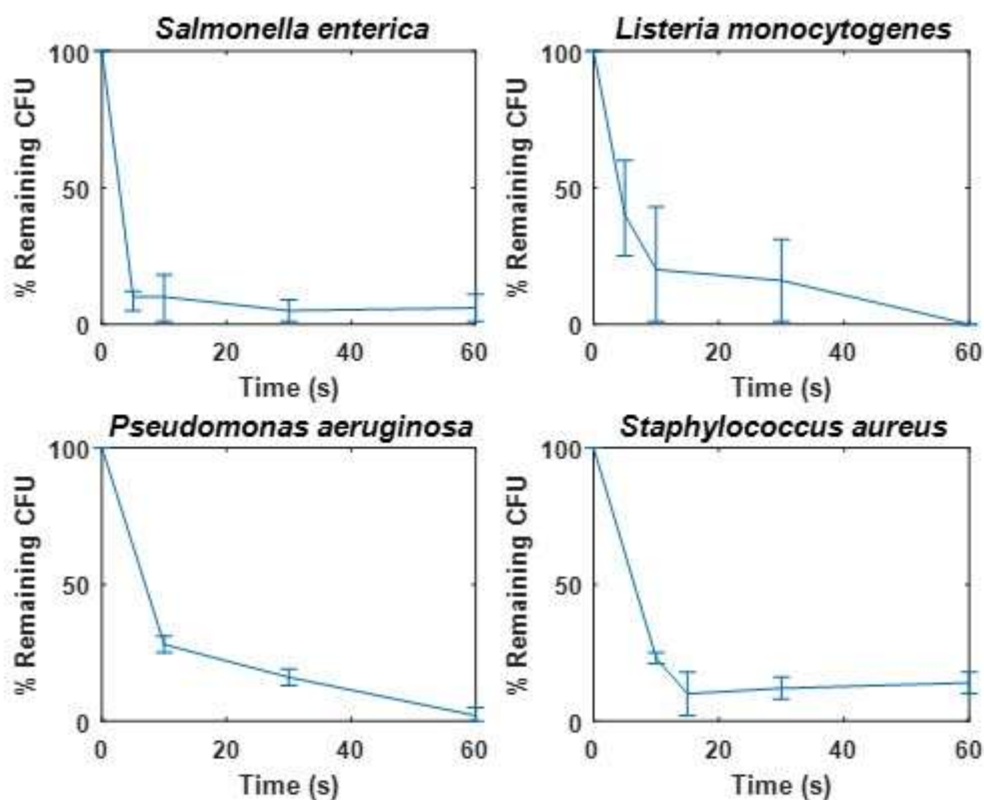

Figure 37. Various organisms CFU counts at specified treatment times at 1800 V and 5 LPM Argon gas flow through single linear discharge. Additional results will be presented in upcoming papers.

The results presented in Fig. 37 are consistent across most substrates tested. These results are tested against controls where the sample is treated with just gas flow and no plasma, and it was found that the impact of the gas flow pushing the bacteria off the substrate is statistically insignificant.

First, every test where oxygen gas and/or atmosphere is the primary flow gas has failed to produce etching. This is the case even when the plasma is run at equivalent or greater power densities to argon plasmas. It has also been extremely difficult to achieve etching with pure argon plasmas. Thus, a potential solution was suggested by Dr. Allen Garner of Purdue University. By hydrating the flow gas with a gas washing bottle or drechsel tube, etching is achieved much more easily. From the work of E. Baek et al and others, it appears that when hydrating the gas, greater quantities of radicals, specifically $^*OH$,O, NO, N_2 and, N_2^+ are formed [35]. This has worked to improve the device's capacity for etching biofilms in single linear discharge devices, but it did not completely remove the inconsistency. For the following experiments, argon gas flows through a 10 mL pipette securely fastened to a 4L PYREX drechsel tube before flowing into the device. A diffuser was initially incorporated in the bottle to further dispense the gas but was removed as it did not yield significant benefits and in fact restricted the gas flow rate to about 8 LPM.

It is important to determine if gas flow affects the biofilm in any way. Fig. 38 shows the effect of flowing hydrated argon gas through an 8x array onto a sample of 2day *P. fluorescens* biofilm. The flow rate of 10.2 LPM is important as it represents the upper end of gas flow rates through an array. Although the gas discolors the biofilm by turning it translucent, it does not serve to remove or displace any native material.

Equivalent flow rates through a single linear discharge do indeed have higher flow densities delivered to the surface, but it has not been found to adversely affect the biofilm. It should be noted that experimentally, the gas flow is turned on slowly with manual control valves, and then the biofilm sample is placed beneath the flow. When using electronic or manual mass flow controllers, there is an initial high pressure burst of

gas before the controller stabilizes. If the sample is already in place when this happens, the biofilm can be blown away if not completely removed.

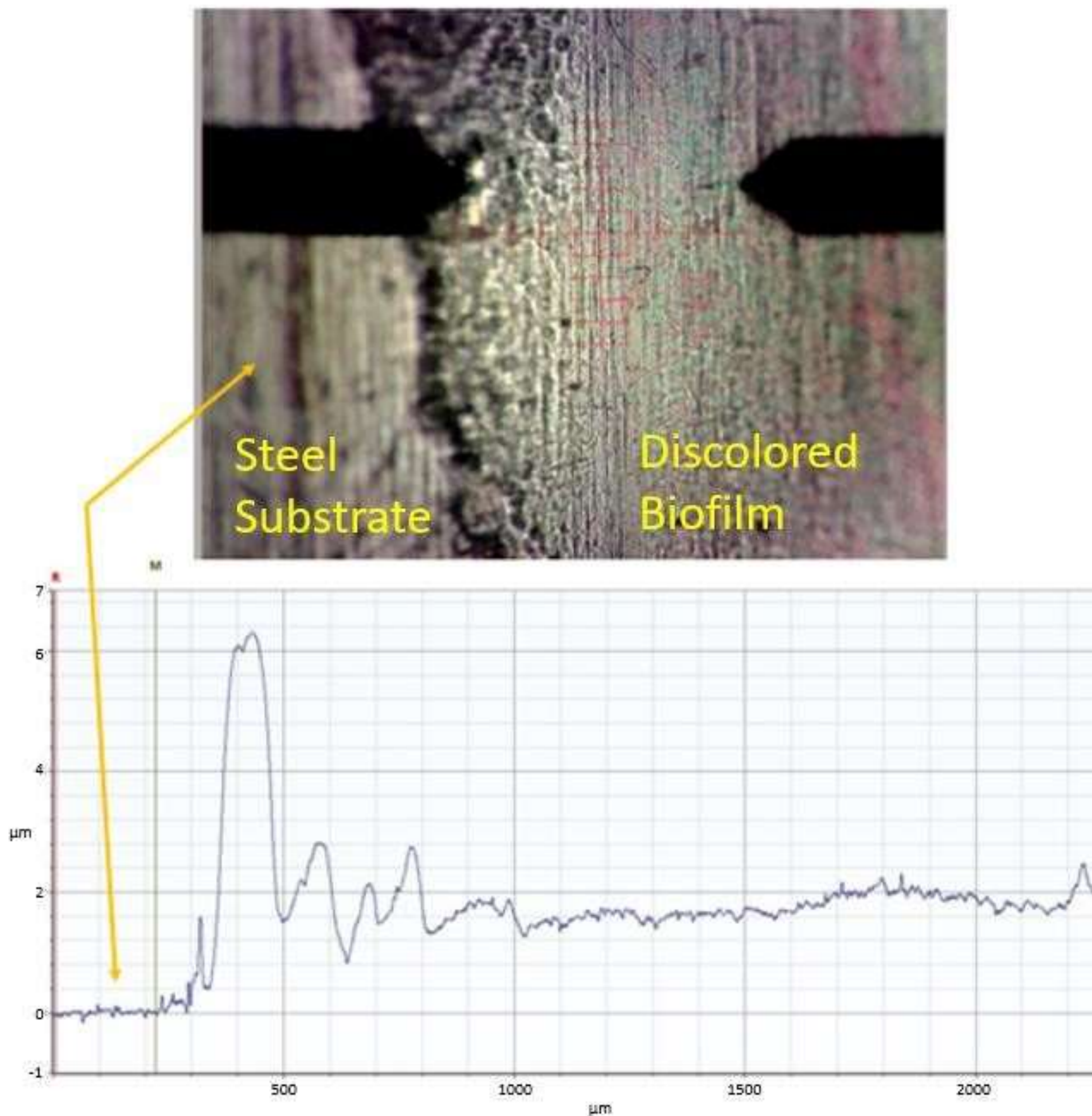

Figure 38. The effect of 10.2 LPM hydrated argon gas flow for 5 minutes through an 8 element array with no plasma. (Top) Microscope image of P. fluorescens on steel. The right hand section is steel substrate and the left shows the discolored bulk biofilm. The yellow arrow points to the areas without biofilm. Clearly, the underlying substrate lines are visible through the biofilm. (Bottom) Profilometer scan of the Top image from left to right. It can be seen that the bulk biofilm is approximately 2 µm even when translucent. This effect only occurs when flowing hydrated gas through the device.

Etching with Single Linear Plasma Discharges

The following represents a summation of experiments that yielded partial and complete etching from single linear discharges. The conditions will be described while noting significant differences when experimental parameters were changed within the same batch of biofilms. These tests are with hydrated flow gas unless noted otherwise.

Fig. 39 shows a control of *P. fluorescens* where no gas and no plasma were flowing. Fig. 40 shows a control test where 8 LPM of Argon is flowed and no plasma. Similar to Fig. 38, left of the yellow arrow is the biofilm turned translucent and right of the arrow is the steel substrate. Notice how the oxygen boundary transitions cleanly into the substrate with minimal dark spots.

Figure 39. P. fluorescens biofilm control with no gas or plasma treatment. The green regions indicate the dried biofilm. The bottom right of the image indicates the steel substrate.

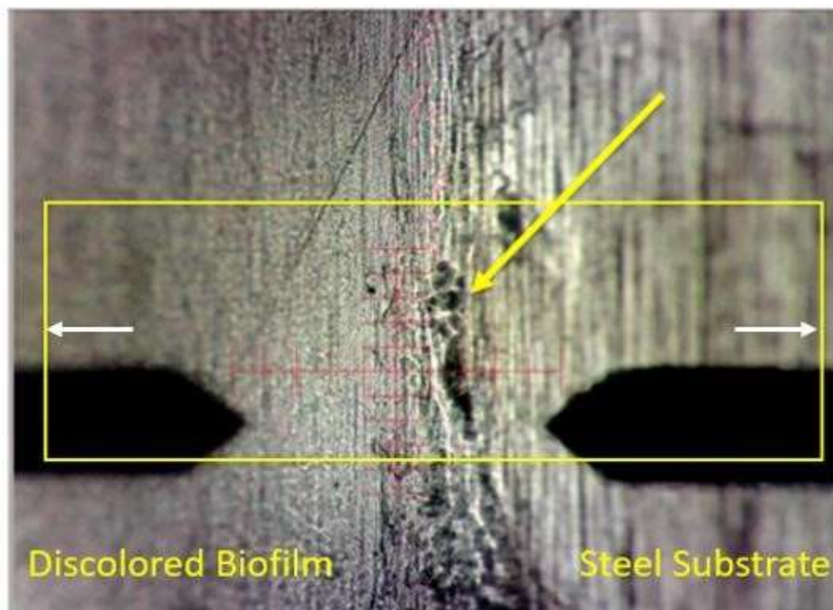

Figure 40. Control test of P. fluorescens with 8 LPM Hydrated Ar for 4 min at 3 mm and no plasma. The large yellow arrow points the boundary between steel substrate on the right and translucent biofilm on the left. The yellow box indicates the orientation of the device above the substrate and outlines a top and bottom boundary of plasma treatment. The plasma discharge above the sample extends off the right and left edges of the box beyond the extent of the image indicated by the small white arrows.

Fig. 41 shows a slide from the same group as Fig. 40 when subjected to equivalent gas flow and duration with a 3100 V plasma operating at 3.1 mA. Note, the plasma device is oriented from right to left directly above the crosshairs. Here it can clearly be seen that removal and displacement of biofilm is occurring. The black spots and ridges indicate deposition of dislodged bacteria, while there are two clear etches down to the substrate. Fig. 42 is a stylus scan starting from the center of the crosshairs moving up towards the darkest black spot. This is interesting in the fact that the etching has only occurred at the thickest part of the biofilm and does not occur in the biofilm bulk. Fig. 43 shows similar results with increasing the gas flow to 9 LPM.

It was thought that since the etching was directly centered beneath the device that more reactive species were deposited directly into this area. However, moving the oxygen

boundary off center and using different spacer designs to more evenly distribute flow gas yielded no change in this etching behavior. It is consistent that at these treatment combinations, the oxygen boundary is the first to be etched away while leaving the bulk biofilm intact. It is possible that the area between the bulk biofilm and oxygen boundary etches first because it experiences the greatest shear forces during incubation from the rotation of the shaker table.

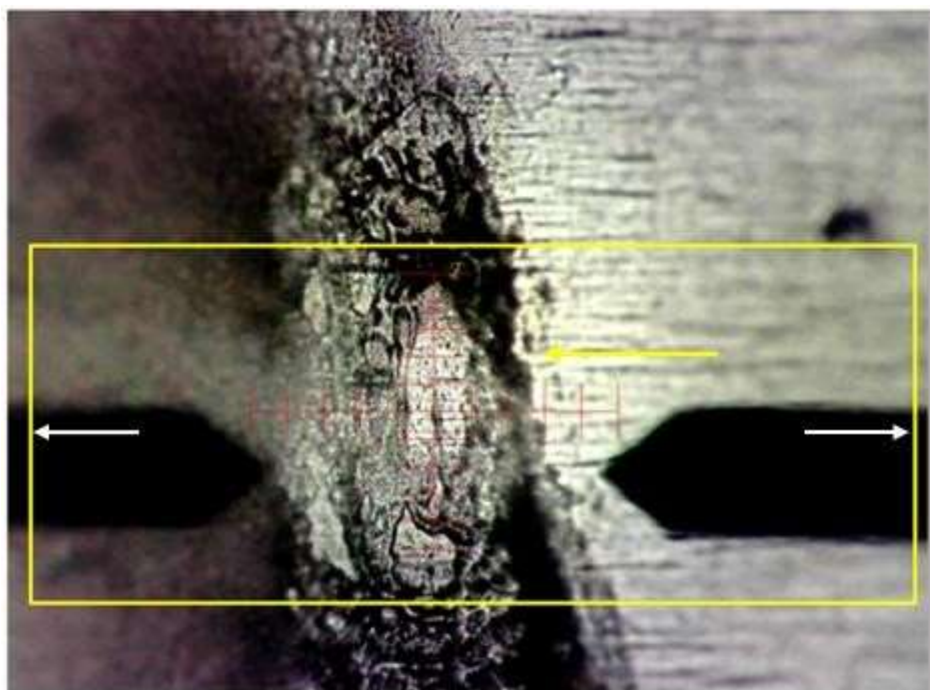

Figure 41. 3100 V, 3.1 mA at 3 mm for 4 min with 8 LPM hydrated Ar. There is significant displacement of biofilm occurring in the oxygen boundary. The bulk biofilm however remains intact. The yellow box indicates the placement of the plasma device over the sample similar to Fig. 40. The device extends off the left and right edges of the box. The yellow arrow indicates the orientation of the scan in Fig. 42.

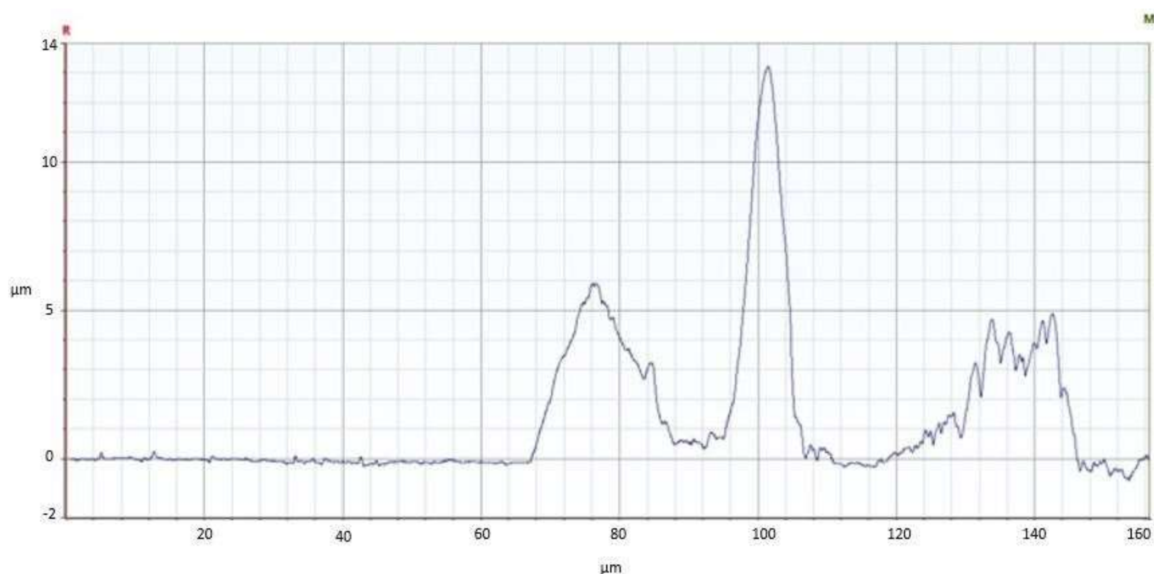

Figure 42. Profilometer scan of Fig. 41. Clearly the first 6 mm is steel substrate before encountering the biofilm oxygen boundary. At 10 mm there is a spike from either biofilm or foreign debris.

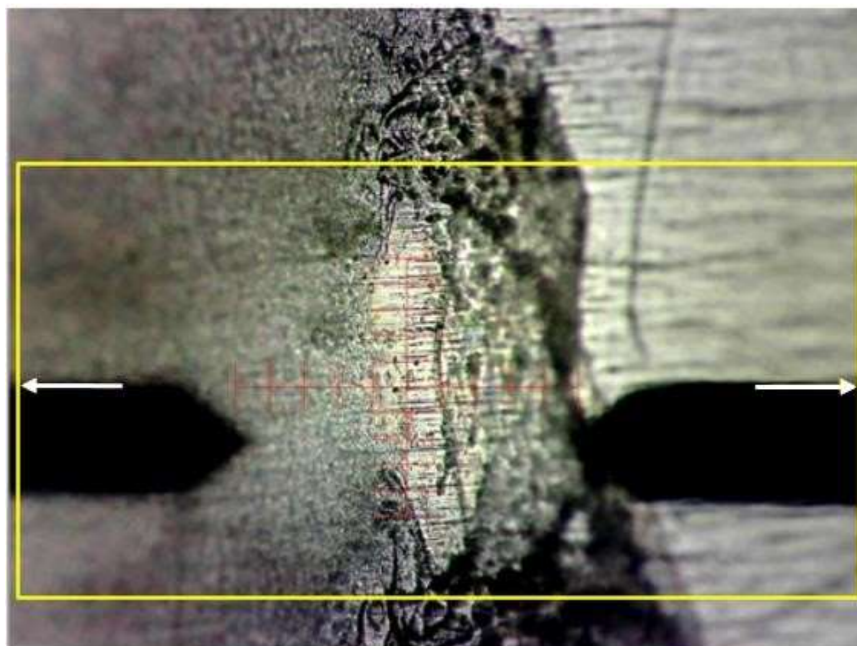

Figure 43. Plasma treatment of 3100 V, 3.1 mA at 3 mm for 4 min with 9 LPM hydrated Ar. The yellow box indicates the placement of the plasma device over the P. fluorescens sample. The device extends off the left and right edges of the box indicated by the small white arrows.

Using the same treatment parameters in Fig. 43, the exposure duration was extended from 4 minutes to 10 minutes. The results are shown in Fig. 44. Obviously, simply extending treatment times do not significantly improve the etching at these treatment conditions.

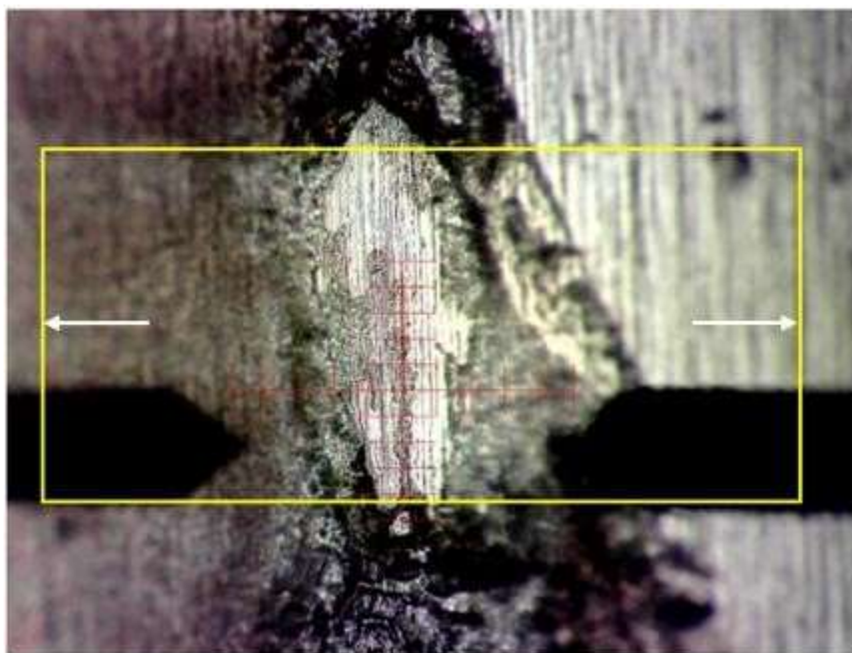

Figure 44. 10 minute treatment at equivalent treatment conditions to that of Fig. 41. The yellow box indicates the orientation of the plasma device above the substrate.

An experiment was then conducted with equivalent conditions to that of Fig. 41 except with the voltage set to 2100 V and 2.1 mA. This result is shown in Fig. 45 and represents a significant breakthrough in ability to etch in the bulk biofilm region. It should be noted that successive duplicates of this experiment have not yielded similar large scale etching. These results do, however, represent an improvement towards the optimal treatment combinations and further testing is necessary. Fig. 46 is a scan from the center of etch in the bulk region upwards. It shows an approximate 4 µm of etching over 4 minutes of treatment.

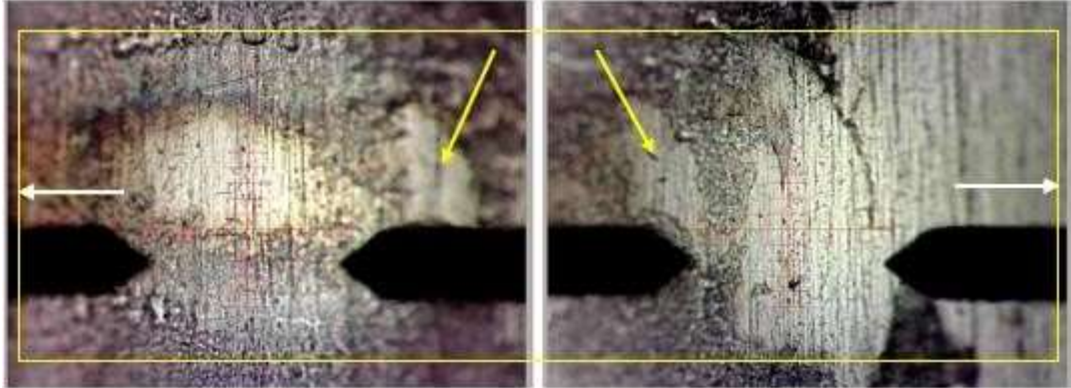

Figure 45. **Etching occurring in the oxygen boundary as well as the bulk regions. (Left) the bulk region shows significant etching. (Right) the etched oxygen boundary has a significantly wider etch area than the bulk. The larger yellow arrows point to the same etch region where the images would overlay. The yellow box indicates the approximate width of the discharge above the sample, extending off the left and right edges of the image indicated by the small white arrows.**

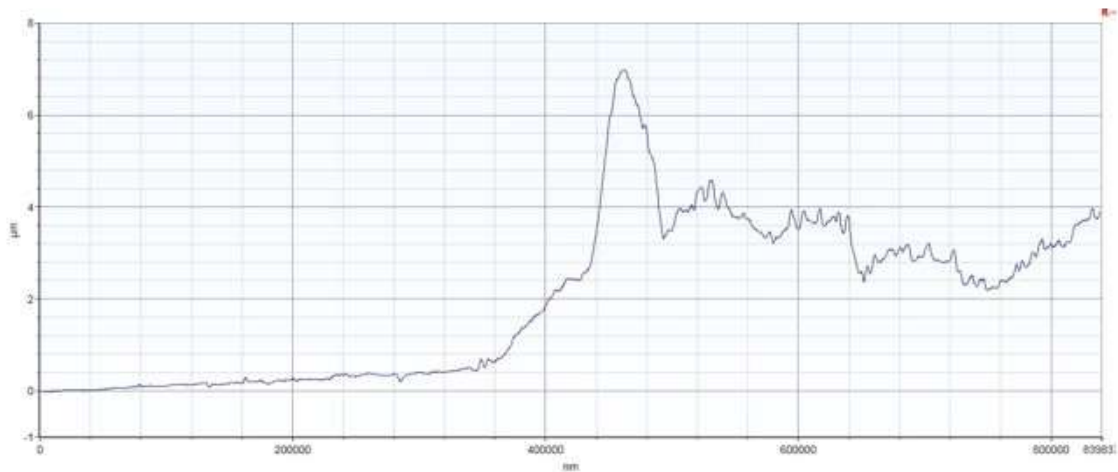

Figure 46. **Scan of Fig. 45 (Left) from the center of the etched region to the top of the figure. This shows an approximate 4 µm of etch over 4 minutes or an etch rate of 1 µm/min.**

Etching with DBD Plasma Arrays

Working in parallel to determining consistent etching with single linear discharges is etching with multi discharge arrays. These array devices have consistently proven to kill bacteria on a variety of substrates, and those results will be presented in future papers. This section will outline the state of development in the DBD array's etching capabilities. The prevailing theory has been that optimizing a single linear discharge device for etching should easily translate into multi discharge devices. However, current results are conflicting in shared treatment conditions, as well as the response from the biofilm. The following describes a set of experiments conducted with an 8x array.

Fig. 47 shows the effects of an 8x array operating at 1600 V, 9.8 mA at 5 mm with 12 LPM of dry Ar gas for 5 minutes with 1 mm gap. From Fig. 47 there are clearly some new and interesting effects. Notably, the oxygen boundary remains intact as opposed to the single discharge devices. It can also be seen that the bulk biofilm has been completely etched away and removed from the surface. This is clear from the striations of scratches on the substrate now being visible. This is significantly different compared to the single linear discharge devices where the oxygen boundary was the first to be etched and the bulk last. Fig. 48 shows the same sample as Fig. 47 with a scan starting from the etched section going into the O_2 boundary.

Fig. 48 shows the extent of the etching ability of the device at these treatment conditions. The coverage area extends the entire width of the substrate coupon which is 19 mm. The total etched area was just under 19 mm^2. This encompasses almost all of the bulk biofilm while leaving a little remaining on the edges. Fig. 49 shows an interesting occurrence where a thicker part of the bulk biofilm remained after treatment but obvious

striation marks occurred. These striations are biofilm built up from the surrounding areas after treatment. They are aligned with the orientation of the device and are mostly linear but it can be seen that they are not perfectly so. Post treatment scans indicate that the etch rate is between 0.5 and 1 μm per minute. This is very small but nonetheless indicates the device's ability to remove biofilms.

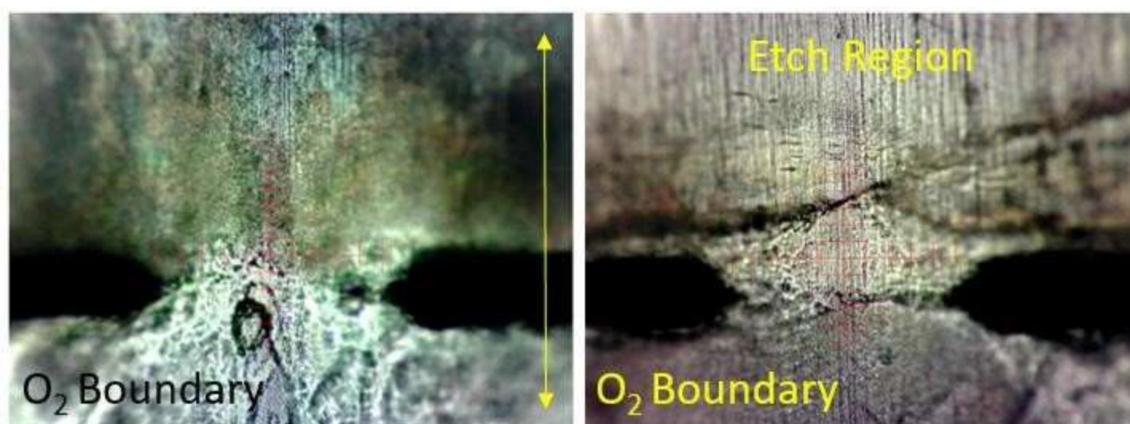

Figure 47. Pre-treatment control and post-treatment of a P. fluorescens biofilm on stainless steel. (Left) Control with 12 LPM of Ar gas for 5 minutes. The oxygen boundary is the bottom of the image and the device is oriented vertically above indicated by the double yellow arrow. (Right) Post-treatment with 1600 V, 9.8 mA at 5 mm with 12 LPM dry Ar for 5 minutes. The etch region is indicated and can clearly be seen as being removed cleaned down to the steel substrate.

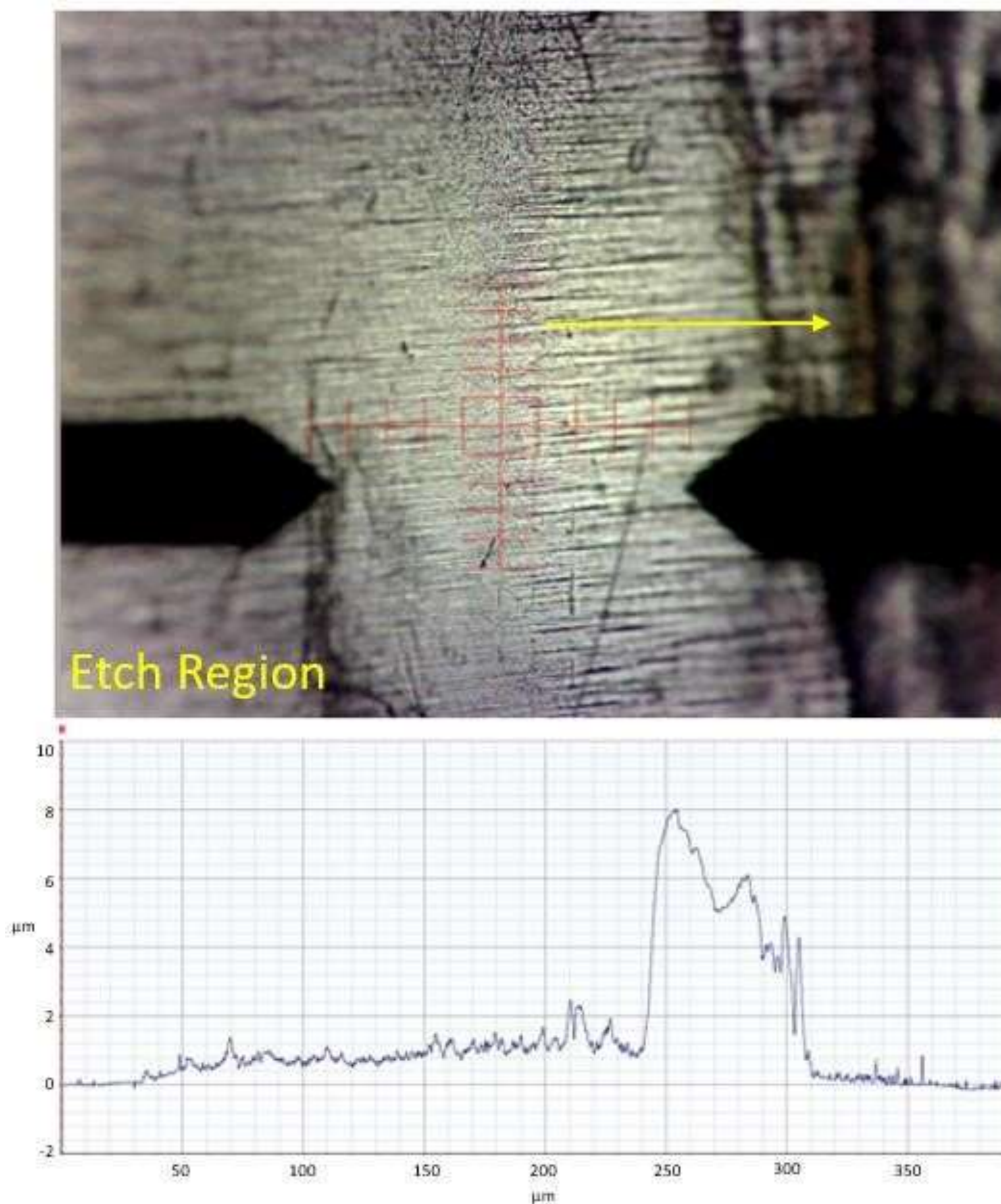

Figure 48. (Top) Image of the scan region described in Fig. 47 starting in the etched biofilm bulk and ending just past the O_2 boundary indicated by the yellow arrow (Left to right). The entire region shown was subjected to plasma treatment. (Bottom) Profilometry scan of the top image from left to right.

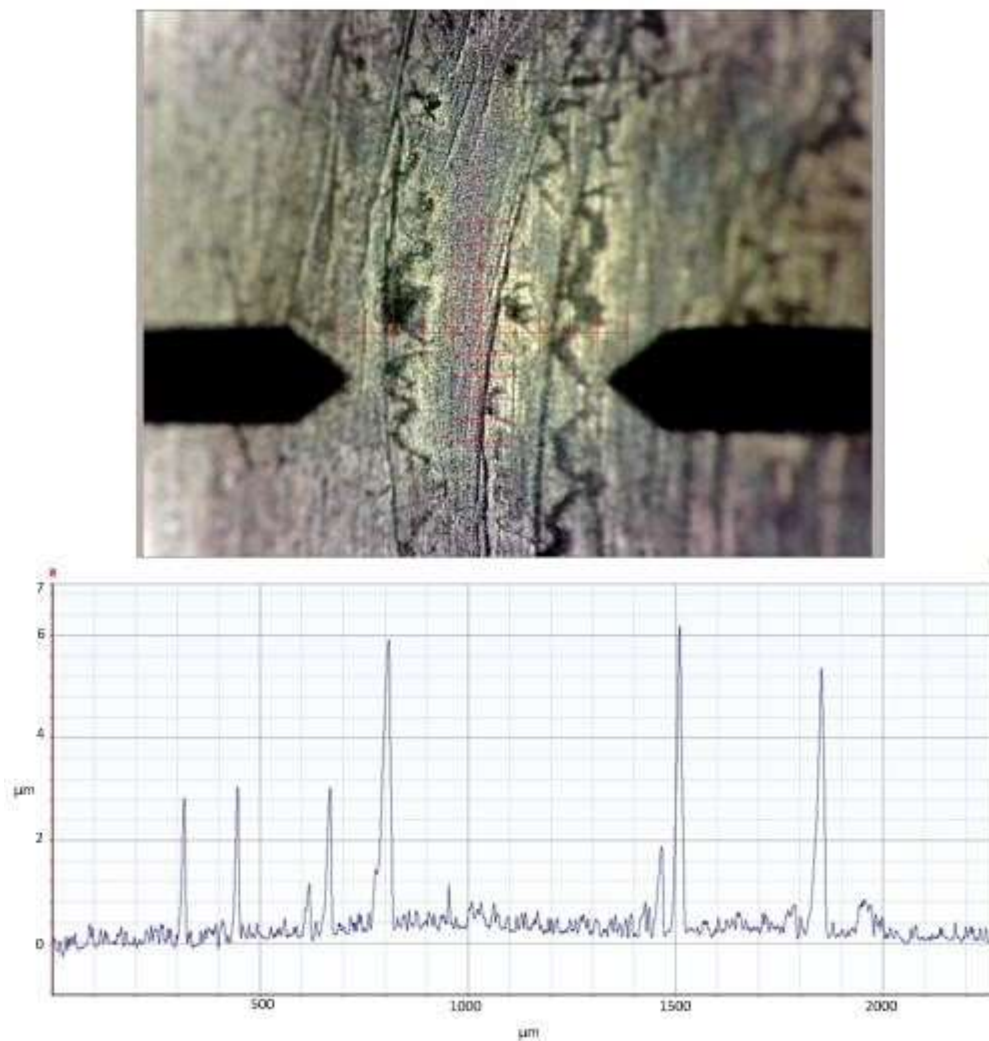

Figure 49. (Top) Striation marks left in the bulk biofilm after treatment outlined in Fig. 47. The spacing of the striations are approximately equal to the width of the plasma discharge in each element. (Bottom) Profilometry scan from right to left across the top image.

CHAPTER 6: SUMMARY AND CONCLUSION

Summary of Results and Discussion

Experiments have shown that uniform CAP dielectric barrier discharges built with LTCC are effective at inactivating a variety of bacterial biofilms and are capable of etching away biofilms. This process remains to be optimized for consistent etching at appreciable rates. It has been shown that arrays produce a more uniform plasma with the incorporation of a 100-200 kΩ ballast resistor. If a discharge channel is misaligned or otherwise defective, it can be detected through external ballast resistor IV characterization. Through refinements in the fabrication process, these devices are reliably produced with failure rates <5%. It is important to note that by placing the ballast resistor on the HV side of the device, the device was able to be moved much closer to the substrate surface. However, it was found that even with the device around 1-2 mm away from the surface, etching was unable to occur.

For single linear discharge devices, etching by reactive species deposition and sputtering mechanisms has occurred at 2100 V and 2.1 mA with 8 LPM of hydrated argon gas for 3 minutes. It has also been found that an 8 element array of discharges etched away *P. fluorescens* by operating at 1600 V, 9.8 mA at 5 mm with 12 LPM of dry Ar gas for 5 minutes with 1 mm gap.

The use of hydrated flow gas is an important parameter in the experiments presented for single linear discharges. So far the only etching that has occurred has been with the use of hydrated flow gas. The reason behind this requirement is as of yet unknown. It is posited that the presence of water vapor increases the presence of

hydroxyl radicals deposited or created on the surface. This suggests that there is a combination of reactive etch and sputtering occurring. From the experiments presented in Chapter 5, it can clearly be seen that the black spots on the sides of the etching area are bacteria physically removed and piled up along the edges of the etch. This indicates the presence of physical sputtering or the formation of etch product. The necessity of including hydrated flow gas suggests that water vapor is an important catalyst in the etching process with single linear discharges. It is concerning that this necessity is not consistent across single linear discharges and multi discharge arrays.

Experimentally, these devices have been shown to kill bacteria in biofilms on a variety of substrates. Stainless steel, plastic, glass and even swine tissue substrates have all demonstrated CFU reductions of > 3-log using 5 minute treatments or less. It has been shown that these devices exhibit the capacity to etch biofilms but are as of yet unreliable by any acceptable statistic. The efficiency is also of concern with approximately 1 μm/min etch rate.

In the results shown in Fig. 45 and Fig. 47, it is interesting to note that lowering the voltage from 3100 V to 2100 V improved the ability to etch in the bulk biofilm. We have actually begun to see that reducing voltage and gas flow levels has had beneficial results. These experiments are currently underway to verify these claims and will be detailed in future papers.

Conclusion

CAP devices have the capacity for greatly improving the sanitation and sterilization capabilities in food processing and medical industries. The devices at Boise State University have been refined over multiple generations of design and fabrication to reliably generate CAP using a capacitive discharge. These devices are capable of treating

large areas by building arrays of single linear discharge devices. The efficacy of killing bacteria in biofilms with these devices has been established over hundreds of tests with multiple organisms on a host of substrates. The ability of these devices to wholly remove biofilms from the substrates has been demonstrated but requires further testing and optimization.

Future Work

Current effort is primarily focused on reliably demonstrating that these devices can etch biofilms on a variety of substrates with standardized treatment settings. This is being accomplished through efforts to optimize the device parameters. Currently, a new generation of high intensity discharges are being developed for the purpose of achieving etch rates on the order of μm/second. Radial devices are being designed for non planar substrates and narrow scalpel devices are being incorporated into bacterial imaging systems for the purpose of dynamically detecting and targeting bacterial biofilms in wound environments. Current high intensity discharges appear promising in achieving high etch rates. These devices could have potential for industrial applications where large scale, fast, chemical free sterilization is desired.

REFERENCES

[1] K. Weltmann and T. von Woedtke, "Plasma medicine—current state of research and medical application", *Plasma Physics and Controlled Fusion*, vol. 59, no. 1, p. 014031, 2016. Available: 10.1088/0741-3335/59/1/014031.

[2] C. Smet, E. Noriega, F. Rosier, J. Walsh, V. Valdramidis and J. Van Impe, "Impact of food model (micro)structure on the microbial inactivation efficacy of cold atmospheric plasma", *International Journal of Food Microbiology*, vol. 240, pp. 47-56, 2017. Available: 10.1016/j.ijfoodmicro.2016.07.024.

[3] J. Lackmann et al., "Photons and particles emitted from cold atmospheric-pressure plasma inactivate bacteria and biomolecules independently and synergistically", *Journal of The Royal Society Interface*, vol. 10, no. 89, 2013. Available: 10.1098/rsif.2013.0591.

[4] B. Park et al., "Sterilization using a microwave-induced argon plasma system at atmospheric pressure", *Physics of Plasmas*, vol. 10, no. 11, pp. 4539-4544, 2003. Available: 10.1063/1.1613655.

[5] E. Kvam, B. Davis, F. Mondello and A. Garner, "Nonthermal Atmospheric Plasma Rapidly Disinfects Multidrug-Resistant Microbes by Inducing Cell Surface Damage", *Antimicrobial Agents and Chemotherapy*, vol. 56, no. 4, pp. 2028-2036, 2012. Available: 10.1128/aac.05642-11.

[6] P. Bruggeman and R. Brandenburg, "Atmospheric pressure discharge filaments and microplasmas: physics, chemistry and diagnostics", *Journal of Physics D: Applied Physics*, vol. 46, no. 46, p. 464001, 2013. Available: 10.1088/00223727/46/46/464001.

[7] D. Millan-Sango et al., "Assessing bacterial recovery and efficacy of cold atmospheric plasma treatments", *Food and Bioproducts Processing*, vol. 96, pp. 154-160, 2015. Available: 10.1016/j.fbp.2015.07.011.

[8] U. Kogelschatz, "Collective phenomena in volume and surface barrier discharges", *Journal of Physics: Conference Series*, vol. 257, p. 012015, 2010. Available: 10.1088/1742-6596/257/1/012015.

[9] N. Philip, B. Saoudi, M. Crevier, M. Moisan, J. Barbeau and J. Pelletier, "The respective roles of UV photons and oxygen atoms in plasma sterilization at reduced gas pressure: the case of N/sub 2/-O/sub 2/ mixtures", *IEEE Transactions on Plasma Science*, vol. 30, no. 4, pp. 1429-1436, 2002. Available: 10.1109/tps.2002.804203.

[10] M. Moreau, N. Orange and M. Feuilloley, "Non-thermal plasma technologies: New tools for bio-decontamination", *Biotechnology Advances*, vol. 26, no. 6, pp. 610-617, 2008. Available: 10.1016/j.biotechadv.2008.08.001.

[11] S. Forghani, M. Ghazali, A. Muchtar, A. Daud, N. Yusoff and C. Azhari, "Effects of plasma spray parameters on TiO2-coated mild steel using design of experiment (DoE) approach", *Ceramics International*, vol. 39, no. 3, pp. 3121-3127, 2012. Available: 10.1016/j.ceramint.2012.09.092.

[12] T. Royintarat, P. Seesuriyachan, D. Boonyawan, E. Choi and W. Wattanutchariya, "Mechanism and optimization of non-thermal plasma-activated water for bacterial inactivation by underwater plasma jet and delivery of reactive species underwater by cylindrical DBD plasma", *Current Applied Physics*, vol. 19, no. 9, pp. 10061014, 2019. Available: 10.1016/j.cap.2019.05.020.

[13] A. Haji, M. Mehrizi and J. Sharifzadeh, "Dyeing of wool with aqueous extract of cotton pods improved by plasma treatment and chitosan: Optimization using response surface methodology", *Fibers and Polymers*, vol. 17, no. 9, pp. 14801488, 2016. Available: 10.1007/s12221-016-6457-0.

[14] N. Misra and C. Jo, "Applications of cold plasma technology for microbiological safety in meat industry", *Trends in Food Science & Technology*, vol. 64, pp. 7486, 2017. Available: 10.1016/j.tifs.2017.04.005.

[15] B. Surowsky, O. Schlüter and D. Knorr, "Interactions of Non-Thermal Atmospheric Pressure Plasma with Solid and Liquid Food Systems: A Review",

Food Engineering Reviews, vol. 7, no. 2, pp. 82-108, 2014. Available: 10.1007/s12393-014-9088-5.

[16] N. Gorbunova, "Low-Temperature Atmospheric-Pressure Plasma in Microbial Decontamination and Meat Technology: A Review", *Theory and Practice of Meat Processing*, vol. 4, no. 1, pp. 21-29, 2019. Available: 10.21323/2414-438x-20194-1-21-29.

[17] C. Du, Y. Liu, Y. Huang, Z. Li, R. Men, Y. Men, and J. Tang, "Qualitation and Quantitation on Microplasma Jet for Bacteria Inactivation," Scientific Reports, vol. 6, no. 1, 2016.

[18] S. Lerouge, A. C. Fozza, M. R. Wertheimer, R. Marchand and L. Yahia, "Sterilization by Low-Pressure Plasma: The Role of Vacuum-Ultraviolet Radiation", Plasmas and Polymers, vol. 5, no. 1, pp. 31-46, 2000.

[19] E. Mintoussov, S. Pendleton, F. Gerbault, N. Popov and S. Starikovskaia, "Fast gas heating in nitrogen–oxygen discharge plasma: II. Energy exchange in the afterglow of a volume nanosecond discharge at moderate pressures", *Journal of Physics D: Applied Physics*, vol. 44, no. 28, p. 285202, 2011. Available: 10.1088/0022-3727/44/28/285202.

[20] K. Cornell, K. Benfield, T.Berntsen, J.Clingerman, A.Croteau, S.Goering, D. Moyer, M.Provost, A.White, D.Plumlee, J.Oxford, and J. Browning, "A Cold Atmospheric Pressure Plasma Discharge Device Exerts Potent Antibiofilm Effects" *Int J Latest Trends Eng Technol*. 2020 Jan; 15(3): 036–041.

[21] S. Schneider et al., "The Role of VUV Radiation in the Inactivation of Bacteria with an Atmospheric Pressure Plasma Jet", *Plasma Processes and Polymers*, vol. 9, no. 6, pp. 561-568, 2012. Available: 10.1002/ppap.201100102.

[22] N. Misra, S. Pankaj, A. Segat and K. Ishikawa, "Cold plasma interactions with enzymes in foods and model systems", *Trends in Food Science & Technology*, vol. 55, pp. 39-47, 2016. Available: 10.1016/j.tifs.2016.07.001.

[23] Finkelnburg W and Maecker H 1956 *Electric Arcs and Thermal Plasmas* (*Encyclopedia of Physics* XXII) ed S Fl¨ugge (Berlin: Springer) p 307

[24] Fridman A 2008 *Plasma Chemistry* (Cambridge: Cambridge University Press)

[25] J. Walsh, J. Shi and M. Kong, "Contrasting characteristics of pulsed and sinusoidal cold atmospheric plasma jets", *Applied Physics Letters*, vol. 88, no. 17, p. 171501, 2006. Available: 10.1063/1.2198100.

[26] K. Malecha, "A PDMS–LTCC bonding using atmospheric pressure plasma for microsystem applications", *Sensors and Actuators B: Chemical*, vol. 181, pp. 486493, 2013. Available: 10.1016/j.snb.2013.01.094.

[27] A. Baker, C. Randall, R. Stewart, R. Fantazier and F. Wise, "Fabrication of a Multilayered Low-Temperature Cofired Ceramic Micro-Plasma-Generating Device", *International Journal of Applied Ceramic Technology*, vol. 3, no. 6, pp. 413-418, 2006. Available: 10.1111/j.1744-7402.2006.02104.x.

[28] A. Hajian et al., "Wet-chemical porosification of LTCC substrates: Dissolution mechanism and mechanical properties", *Microporous and Mesoporous Materials*, vol. 288, p. 109593, 2019. Available: 10.1016/j.micromeso.2019.109593.

[29] C. Schulz, T. Styrnoll, R. Storch, P. Awakowicz, T. Musch and I. Rolfes, "The Multipole Resonance Probe: Progression and Evaluation of a Process Compatible Plasma Sensor", *IEEE Sensors Journal*, vol. 14, no. 10, pp. 3408-3417, 2018. Available: 10.1109/jsen.2014.2333659.

[30] P. Bembnowicz et al., "Preliminary studies on LTCC based PCR microreactor", *Sensors and Actuators B: Chemical*, vol. 150, no. 2, pp. 715-721, 2010. Available: 10.1016/j.snb.2010.08.015.

[31] A. Baker et al., "Integration Concepts for the Fabrication of LTCCStructures", *International Journal of Applied Ceramic Technology*, vol. 2, no. 6, pp. 514-520, 2005. Available: 10.1111/j.1744-7402.2005.02052.x.

[32] K. Malecha and L. Golonka, "Microchannel fabrication process in LTCC ceramics", *Microelectronics Reliability*, vol.48, no.6, pp. 866-871, 2008. Available: 10.1016/j.microrel.2008.03.013.

[33] F. Barlow et al., "Fabrication of Precise Fluidic Structures in LTCC", *International Journal of Applied Ceramic Technology*, vol. 6, no. 1, pp. 18-23, 2009. Available: 10.1111/j.1744-7402.2008.02315.x.

[34] GreenTape™ 9K7 LTCC System: Low Temperature Co-fired Ceramic," Dupont Electronic Solutions. [Online]. Available: https://www.dupont.com/products/green-tape-9k7-ltcc-material-system.html

[35] E. Baek, H. Joh, S. Kim and T. Chung, "Effects of the electrical parameters and gas flow rate on the generation of reactive species in liquids exposed to atmospheric pressure plasma jets", *Physics of Plasmas*, vol. 23, no. 7, p. 073515, 2016. Available: 10.1063/1.4959174.